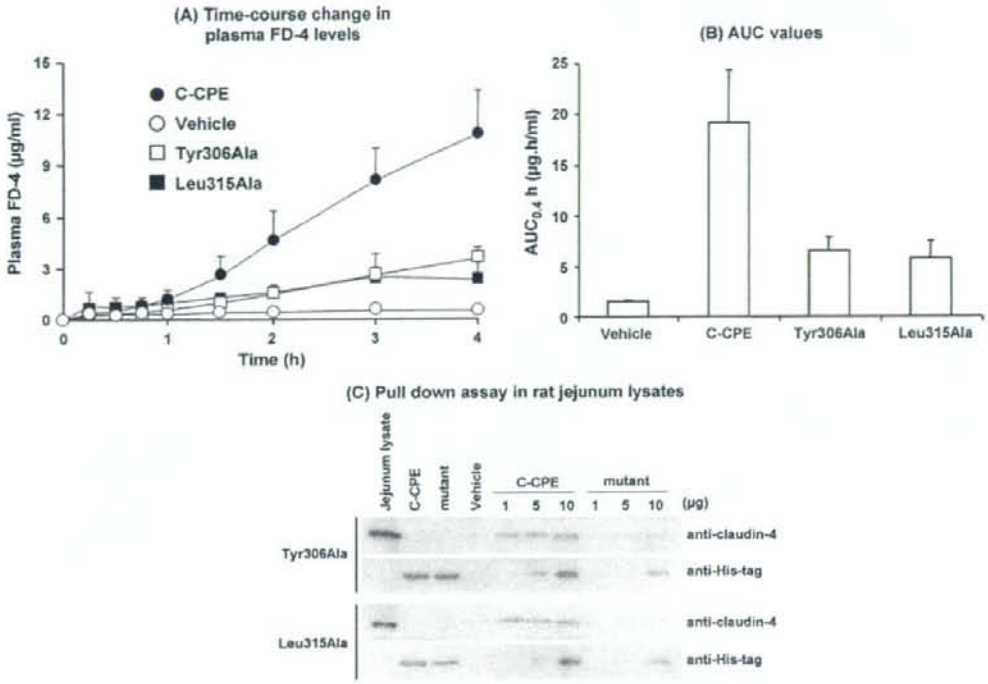

Fig. 2 – Role of Leu315 in the enhancement of absorption by C-CPE in rat jejunum. (A and B) Enhancement of jejunal absorption of FD-4 by C-CPE. The enhancement of absorption by mutant C-CPEs was evaluated by an *in situ* loop assay using rat jejunum. Briefly, rat jejunum was treated with FD-4 (10 mg/ml) in the presence of vehicle, C-CPE (0.2 mg/ml), or mutated C-CPE (0.2 mg/ml). The plasma FD-4 levels were determined at the indicated time (A), and the $AUC_{0-4\ h}$ values were calculated (B). Values are means ± S.E.M. ($n = 4$). (C) Pull-down assay in rat jejunum lysate. Mucosal epithelium in rat jejunum was recovered with a scraper and lysed in lysis buffer as described in Section 2. The lysates were incubated with C-CPE or mutated C-CPE for 30 min at 37 °C. Next, Ni-NTA agarose was added, and after a 3-h incubation at 4 °C, the precipitated Ni-NTA agarose was separated by SDS-PAGE and analyzed by Western blotting. The results are representative of three independent experiments.

[32]. We therefore examined the effect of Tyr306Ala and Leu315Ala on rat jejunal absorption of FD-4. As shown in Fig. 2A and B, C-CPE enhanced the absorption of FD-4 (12.2-fold compared to vehicle-treated controls), and Tyr306Ala and Leu315Ala had reduced abilities to enhance jejunal absorption (4.2- and 3.7-fold compared to vehicle-treated controls, respectively). To further evaluate the interaction of mutated C-CPEs with rat claudin-4, we performed a pull-down assay using rat jejunal lysate. Much less claudin-4 was precipitated by the Tyr306Ala and Leu315Ala mutants than by C-CPE, indicating that these two mutants have lower affinities for rat claudin-4 than C-CPE (Fig. 2C).

3.3. *The combination of Tyr306 and Leu315 is important for C-CPE modulation of claudin-4*

We found that ability of C-CPE to modulate claudin-4 is partially reduced by substitution of Tyr306 or Leu315 with alanine (Fig. 1 and Tables 3 and 4). We therefore evaluated whether the Leu315Ala mutation has synergistic effects by preparing double mutants Tyr306Ala/Leu315Ala, Tyr310Ala/Leu315Ala, and Tyr312Ala/Leu315Ala. Claudin-4 was precipitated by addition of Leu315Ala at 5 μg/ml but not by any of the double-alanine mutants at 10 μg/ml (Fig. 3A). Also, the double-substituted mutants did not affect C-CPE-PSIF-induced cytotoxicity even at 10 μg/ml (Fig. 3B), indicating that they lost their affinity for claudin-4.

Next, we investigated the absorption-enhancing effects of the double mutated C-CPEs using an *in situ* loop assay. Replacement of Tyr306 or Leu315 by alanine partially reduced the enhancement of absorption (Fig. 2A and B), whereas C-CPE with a combination of Leu315Ala and either Tyr306Ala, Tyr310Ala, or Tyr312Ala lost its absorption-enhancing effect (Fig. 4A and B). Similar results were obtained in the TEER assay using Caco-2 monolayers. Reduction of TEER was not observed for these double-substituted mutants (Fig. 4C). These data indicate that in addition to Tyr306, Leu315 is a key residue determining the potency of C-CPE as a modulator of the TJ barrier.

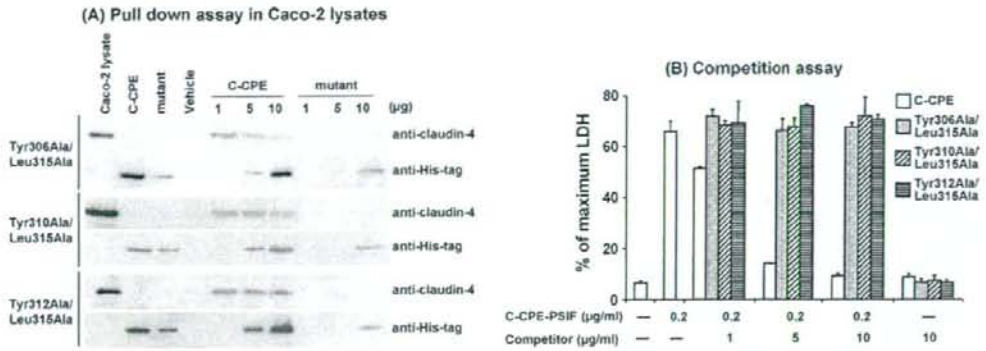

Fig. 3 – Interaction between double-substituted mutant C-CPE and claudin-4. Interaction of double-substituted mutant C-CPEs (Tyr306Ala/Leu315Ala, Tyr310Ala/Leu315Ala, and Tyr312Ala/Leu315Ala) with claudin-4 was evaluated by a pull-down assay using Caco-2 cell lysates (A) and by competitive inhibition of C-CPE-PSIF-induced cytotoxicity in CL4/L cells (B) as described in Fig. 1A and B, respectively. The results are representative of three independent experiments. In panel B, values are means ± S.D. ($n = 3$).

4. Discussion

Claudin is a promising target for developing a drug delivery system via the paracellular route. Our previous findings indicated that C-CPE is a potent modulator of claudin-4 and that the C-terminal 16 amino acids are pivotal for modulation of claudin-4 by C-CPE [32,38]. We have also evaluated the role of tyrosine residues within these 16 C-terminal amino acids by alanine scanning [33,39]. In the present study, we carried out a systematic functional domain mapping of these 16 amino acid residues. We found that Leu315 in addition to Tyr306 is pivotal for the interaction between C-CPE and claudin-4 and for modulation of the TJ barrier by C-CPE.

Functional domain mapping is needed for the development of claudin modulators based on C-CPE. We therefore screened for residues involved in binding of C-CPE to claudin-4 by a competition assay. We found that some mutants, such as Ser307Ala and Lys318Ala, had a slightly higher affinity for claudin-4 than C-CPE (Table 3). We did not focus on these mutants in the current studies, but it will be interesting to examine this further in future studies. We also found that substitution of Ser307 or Lys318 with alanine did not affect the abilities of C-CPE to modulate the TJ barrier and interact with claudin-4 in a pull-down assay (Table 4 and data not shown, respectively). Thus, at least, Ser307 and Lys318 do not appear to be essential for the activities of C-CPE. The results of our systematic domain mapping studies of the C-terminal 16 amino acids in C-CPE from the current study and from our previous report are summarized in Table 5 [33,38]. They suggest that multiple residues in C-CPE, especially Tyr306 and Leu315, are critical for the modulation of claudin-4.

Like Tyr306Ala, the Leu315Ala mutant had the reduced abilities to bind claudin-4, modulate the TJ barrier, and enhance absorption compared to those of C-CPE. The precise mechanism by which C-CPE disrupts the TJ barrier is still unclear. Sonoda et al. found that treatment of MDCK cells with C-CPE caused the disappearance of claudin-4 from TJs and a decrease in intracellular claudin-4 protein levels, indicating that claudin-4 may be degraded after its interaction with C-CPE [31]. Claudin-4 contains a signal sequence for sorting to clathrin-coated vesicles (a ALGVLL motif at amino acids 92–97 and a YVGW motif at amino acids 165–168) [40,41]. It is possible that C-CPE-bound claudin-4 is taken up by clathrin-mediated endocytosis. Indeed, Matsuda et al. showed that endocytosis of claudins occurs during the remodeling of TJs [42].

Do Tyr306 and Leu315 have the same function? Substitution of Tyr306 or Leu315 in C-CPE with alanine resulted in a partial reduction in the ability of C-CPE to modulate claudin-4, and the effects of double alanine-substitution were

Table 5 – Summary of functional domain mapping in the C-terminal 16 amino acids of C-CPE

Amino acid residue	Binding to claudin	Modulation of TJ barrier	Jejunal absorption	Source
Tyr306	Yes	Yes	Yes	This study, Harada et al. [33]
Tyr310	Yes	No	No	Harada et al. [33]
Tyr312	Yes	No	Yes	Harada et al. [33]
Leu315	Yes	Yes	Yes	This study

Binding to claudin was assessed using a competition assay using C-CPE-PSIF, modulation of TJ barrier was determined using a TEER assay using Caco-2 monolayer, and jejunal absorption based on an in situ loop assay using rat jejunum. Yes and No indicate important and not important for each function of C-CPE, respectively.

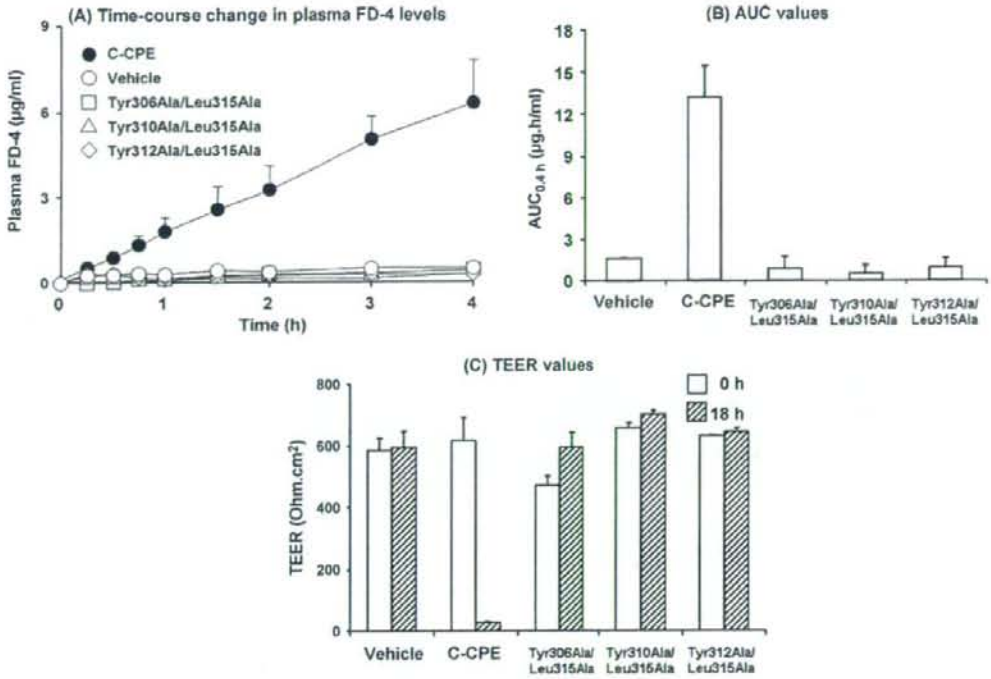

Fig. 4 – Modulation of TJ barrier by double-substituted mutant C-CPEs. (A and B) Enhancement of absorption by double-mutated C-CPEs in rat jejunum. Time-course of plasma FD-4 levels (A) and $AUC_{0-4\,h}$ values (B) were evaluated as described in Fig. 2A and B. Values are means ± S.E.M. (n = 4). (C) TEER assay in Caco-2 monolayer cells. Caco-2 cells were grown on Transwell™ filters. After TJs were developed, vehicle, C-CPE or mutated C-CPEs was added at 20 μg/ml, and TEER values were measured after 0 and 18 h. Values are means ± S.D. (n = 4).

additive (Fig. 4), suggesting that these two residues interact with claudin-4 at different sites or in different ways. Substitution of Tyr306 with Phe (aromatic and hydrophobic residue) and Trp (aromatic, hydrophobic, and polar residue) but not Lys (polar and cationic residue) did not affect the binding of C-CPE to claudin-4 or the modulation of the TJ barrier [39]. Taken together, these findings suggest that C-CPE interact with claudin-4 on the membrane through a hydrophobic cluster formed by the side-chains of Tyr at position 306 and Leu at position 315. Double substitution of Leu315 and Tyr310 or Tyr312 with alanine caused a loss of activities, indicating that the two residues equally and cooperatively contribute to modulation of claudin-4 by C-CPE. Indeed, triple- or quadruple-alanine mutants at Tyr306, Tyr310, Tyr312, and Leu315 lack activities like the double mutants (data not shown).

Other than the functional analyses of C-CPE, little is known about mode of action of C-CPE as a claudin modulator. Determination of the three-dimensional structure of claudin and C-CPE/CPE should help elucidate the mechanism by which C-CPE modulates claudin-4, but the tertiary structures of claudin and CPE have not yet been solved. Very recently, Van Itallie et al. reported structure of the C-terminal claudin-binding domain of CPE [43]. The structure has a nine strand β sandwich, and the claudin-4-binding site is on a loop domain between β8 and β9 strands. Tyr306, Tyr310 and Tyr312 exist on the loop domain, and Leu315 exists in the β9 strand. Our data is consistent with the putative claudin-4-binding domain by the structural analysis.

In conclusion, we carried out the complete fine mapping of the C-terminal 16 amino acids of C-CPE to determine their roles in claudin-4 modulation. We found that Leu315 plays a pivotal role in the modulation of claudin-4 by C-CPE. Together, our previous and current results indicate that Tyr at positions 306, 310, and 312 and Leu at position 315 of C-CPE participate in the modulation of claudin-4. These findings should help in the development of a novel claudin modulator based on C-CPE.

Acknowledgements

We thank Y. Hattori, A. Koyama, and A. Itoh for their kind support. We thank Drs. S. Tsukita and M. Furuse for providing us with CL4/L cells. This study was partly supported by a Grant-in-Aid from the Ministry of Education, Science, and Culture of Japan, Mochida Memorial Foundation for Medical and Pharmaceutical Sciences, Takeda Science Foundation,

Cosmetology Research Foundation, Shiseido Grant for Scientific Research, Tokyo Biochemical Research Foundation, Senri Life Science Foundation, and Astellas Foundation for Research on Metabolic Disorders.

REFERENCES

[1] White RE. High-throughput screening in drug metabolism and pharmacokinetic support of drug discovery. Annu Rev Pharmacol Toxicol 2000;40:133–57.
[2] Roberts SA. High-throughput screening approaches for investigating drug metabolism and pharmacokinetics. Xenobiotica 2001;31:557–89.
[3] Majumdar S, Duvvuri S, Mitra AK. Membrane transporter/receptor-targeted prodrug design: strategies for human and veterinary drug development. Adv Drug Deliv Rev 2004;56:1437–52.
[4] Mizuno N, Niwa T, Yotsumoto Y, Sugiyama Y. Impact of drug transporter studies on drug discovery and development. Pharmacol Rev 2003;55:425–61.
[5] Inui KI, Masuda S, Saito H. Cellular and molecular aspects of drug transport in the kidney. Kidney Int 2000;58:944–58.
[6] Koepsell H. Organic cation transporters in intestine, kidney, liver, and brain. Annu Rev Physiol 1998;60:243–66.
[7] Meijer DK, Hooiveld GJ, Schinkel AH, van Montfoort JE, Haas M, de Zeeuw D, et al. Transport mechanisms for cationic drugs and proteins in kidney, liver and intestine: implication for drug interactions and cell-specific drug delivery. Nephrol Dial Transplant 1999;14(Suppl. 4):1–3.
[8] Van Aubel RA, Masereeuw R, Russel FG. Molecular pharmacology of renal organic anion transporters. Am J Physiol 2000;279:F216–32.
[9] Powell DW. Barrier function of epithelia. Am J Physiol 1981;241:G275–88.
[10] Anderson JM, Van Itallie CM. Tight junctions and the molecular basis for regulation of paracellular permeability. Am J Physiol 1995;269:G467–75.
[11] Tidball CS, Lipman RI. Enhancement of jejunal absorption of heparinoid by sodium ethylenediaminetetraacetate in the dog. Proc Soc Exp Biol Med 1962;111:713–5.
[12] Engel RH, Riggi SJ. Effect of sulfated and sulfonated surfactants on the intestinal absorption of heparin. Proc Soc Exp Biol Med 1969;130:879–84.
[13] Aungst BJ. Intestinal permeation enhancers. J Pharm Sci 2000;89:429–42.
[14] Hochman J, Artursson P. Mechanisms of absorption enhancement and tight junction regulation. J Control Release 1994;29:253–67.
[15] Yamamoto A, Uchiyama T, Nishikawa R, Fujita T, Muranishi S. Effectiveness and toxicity screening of various absorption enhancers in the rat small intestine: effects of absorption enhancers on the intestinal absorption of phenol red and the release of protein and phospholipids from the intestinal membrane. J Pharm Pharmacol 1996;48:1285–9.
[16] Kondoh M, Takahashi A, Fujii M, Yagi K, Watanabe Y. A novel strategy for a drug delivery system using a claudin modulator. Biol Pharm Bull 2006;29:1783–9.
[17] Van Itallie CM, Anderson JM. Claudins and epithelial paracellular transport. Annu Rev Physiol 2006;68:403–29.
[18] Furuse M, Tsukita S. Claudins in occluding junctions of humans and flies. Trends Cell Biol 2006;16:181–8.
[19] Furuse M, Fujita K, Hiiragi T, Fujimoto K, Tsukita S. Claudin-1 and -2: novel integral membrane proteins localizing at tight junctions with no sequence similarity to occludin. J Cell Biol 1998;141:1539–50.
[20] Morita K, Furuse M, Fujimoto K, Tsukita S. Claudin multigene family encoding four-transmembrane domain protein components of tight junction strands. Proc Natl Acad Sci USA 1999;96:511–6.
[21] Simon DB, Lu Y, Choate KA, Velazquez H, Al-Sabban E, Praga M, et al. Paracellin-1, a renal tight junction protein required for paracellular Mg^{2+} resorption. Science 1999;285:103–6.
[22] Turksen K, Troy TC. Claudin-6: a novel tight junction molecule is developmentally regulated in mouse embryonic epithelium. Dev Dyn 2001;222:292–300.
[23] Furuse M, Hata M, Furuse K, Yoshida Y, Haratake A, Sugitani Y, et al. Claudin-based tight junctions are crucial for the mammalian epidermal barrier: a lesson from claudin-1-deficient mice. J Cell Biol 2002;156:1099–111.
[24] Nitta T, Hata M, Gotoh S, Seo Y, Sasaki H, Hashimoto N, et al. Size-selective loosening of the blood–brain barrier in claudin-5-deficient mice. J Cell Biol 2003;161:653–60.
[25] Furuse M, Sasaki H, Tsukita S. Manner of interaction of heterogeneous claudin species within and between tight junction strands. J Cell Biol 1999;147:891–903.
[26] Furuse M, Furuse K, Sasaki H, Tsukita S. Conversion of zonulae occludentes from tight to leaky strand type by introducing claudin-2 into Madin-Darby canine kidney I cells. J Cell Biol 2001;153:263–72.
[27] Horiguchi Y, Uemura T, Kamata Y, Kozaki S, Sakaguchi G. Production and characterization of monoclonal antibodies to *Clostridium perfringens* enterotoxin. Infect Immun 1986;52:31–5.
[28] Hanna PC, Mietzner TA, Schoolnik GK, McClane BA. Localization of the receptor-binding region of *Clostridium perfringens* enterotoxin utilizing cloned toxin fragments and synthetic peptides. The 30 C-terminal amino acids define a functional binding region. J Biol Chem 1991;266:11037–43.
[29] Hanna PC, Wieckowski EU, Mietzner TA, McClane BA. Mapping of functional regions of *Clostridium perfringens* type A enterotoxin. Infect Immun 1992;60:2110–4.
[30] Katahira J, Inoue N, Horiguchi Y, Matsuda M, Sugimoto N. Molecular cloning and functional characterization of the receptor for *Clostridium perfringens* enterotoxin. J Cell Biol 1997;136:1239–47.
[31] Sonoda N, Furuse M, Sasaki H, Yonemura S, Katahira J, Horiguchi Y, et al. *Clostridium perfringens* enterotoxin fragment removes specific claudins from tight junction strands: evidence for direct involvement of claudins in tight junction barrier. J Cell Biol 1999;147:195–204.
[32] Kondoh M, Masuyama A, Takahashi A, Asano N, Mizuguchi H, Koizumi N, et al. A novel strategy for the enhancement of drug absorption using a claudin modulator. Mol Pharmacol 2005;67:749–56.
[33] Harada M, Kondoh M, Ebihara C, Takahashi A, Komiya E, Fujii M, et al. Role of tyrosine residues in modulation of claudin-4 by the C-terminal fragment of *Clostridium perfringens* enterotoxin. Biochem Pharmacol 2007;73:206–14.
[34] Ebihara C, Kondoh M, Hasuike N, Harada M, Mizuguchi H, Horiguchi Y, et al. Preparation of a claudin-targeting molecule using a C-terminal fragment of *Clostridium perfringens* enterotoxin. J Pharmacol Exp Ther 2006;316:255–60.
[35] Sallee VL, Wilson FA, Dietschy JM. Determination of unidirectional uptake rates for lipids across the intestinal brush border. J Lipid Res 1972;13:184–92.

[36] Utoguchi N, Watanabe Y, Shida T, Matsumoto M. Nitric oxide donors enhance rectal absorption of macromolecules in rabbits. Pharm Res 1998;15:870–6.
[37] Ohtake K, Natsume H, Ueda H, Morimoto Y. Analysis of transient and reversible effects of poly-L-arginine on the in vivo nasal absorption of FITC-dextran in rats. J Control Release 2002;82:263–75.
[38] Takahashi A, Kondoh M, Masuyama A, Fujii M, Mizuguchi H, Horiguchi Y, et al. Role of C-terminal regions of the C-terminal fragment of *Clostridium perfringens* enterotoxin in its interaction with claudin-4. J Control Release 2005;108:56–62.
[39] Ebihara C, Kondoh M, Harada M, Fujii M, Mizuguchi H, Tsunoda S, et al. Role of Tyr306 in the C-terminal fragment of *Clostridium perfringens* enterotoxin for modulation of tight junction. Biochem Pharmacol 2007;73:824–30.
[40] Bonifacino JS, Traub LM. Signals for sorting of transmembrane proteins to endosomes and lysosomes. Annu Rev Biochem 2003;72:395–447.
[41] Ivanov AI, Nusrat A, Parkos CA. Endocytosis of epithelial apical junctional proteins by a clathrin-mediated pathway into a unique storage compartment. Mol Biol Cell 2004;15:176–88.
[42] Matsuda M, Kubo A, Furuse M, Tsukita S. A peculiar internalization of claudins, tight junction-specific adhesion molecules, during the intercellular movement of epithelial cells. J Cell Sci 2004;117:1247–57.
[43] Van Itallie CM, Betts L, Smedley 3rd JG, McClane BA, Anderson JM. Structure of the claudin-binding domain of *Clostridium perfringens* enterotoxin. J Biol Chem 2008;283:268–74.

Hepatoprotective Effect of Vitamin B_{12} on Dimethylnitrosamine-Induced Liver Injury

Katsuhiro ISODA,[a] Noritaka KAGAYA,[a] Soichiro AKAMATSU,[a] Shinji HAYASHI,[a] Makoto TAMESADA,[b] Aiko WATANABE,[b] Masakazu KOBAYASHI,[b] Yoh-ichi TAGAWA,[c] Masuo KONDOH,[a] Masaya KAWASE,[d] and Kiyohito YAGI*,[a]

[a] *Graduate School of Pharmaceutical Sciences, Osaka University; 1–6 Yamada-oka, Suita, Osaka 565–0871, Japan:* [b] *Research and Development Center, Kobayashi Pharmaceutical Co., Ltd.; 1–30–3 Toyokawa, Ibaraki, Osaka 567–0057, Japan:* [c] *Department of Biomolecular Engineering, Graduate School of Bioscience and Biotechnology, Tokyo Institute of Technology; 4259 Nagatsuta-cho, Yokohama, Kanagawa 226–8501, Japan: and* [d] *Faculty of Pharmaceutical Sciences, Osaka-Ohtani University; 3–11–1 Nishikiori-kita, Tondabayashi, Osaka 584–8540, Japan.*

Received August 21, 2007; accepted November 9, 2007; published online November 19, 2007

Vitamin B_{12} contains a cobalt complex and accumulates at high levels in the liver. Vitamin B_{12} was examined for its hepatoprotective effect on dimethylnitrosamine-induced liver injury in mice. Vitamin B_{12} decreased the blood levels of aspartate aminotransferase and alanine aminotransferase, and clearly inhibited the overaccumulation of collagen fibrils. Reverse transcription-polymerase chain reaction (RT-PCR) analysis of the liver showed that the gene expression of α-smooth muscle actin and heat-shock protein 47, which are markers of fibrosis, were suppressed by vitamin B_{12} administration. Our findings indicate that vitamin B_{12} could be an effective hepatoprotective agent.

Key words hepatoprotection; vitamin B_{12}; liver fibrosis; metal complex

The incidence of hepatoma related to hepatitis C and B continues to increase in developed countries. Chronic liver injury, including that caused by virus infection, cause persistent inflammation and fibrosis, followed by the development of liver cirrhosis and hepatoma. The use of interferon (IFN) has become the first-line treatment for viral hepatitis, but it is not effective in patients with a high viral load. Recently, investigators have begun to seek hepatoprotective agents that might facilitate the treatment of liver failure.

Vitamin B_{12} contains a cobalt complex and is therefore also known as cobalamin.[1] Its molecular weight is the largest of all the vitamins, and it is known to accumulate at high levels in the liver. Therefore, the concentration of vitamin B_{12} in the blood rises in the presence of acute or chronic liver disease.[2,3] Also, vitamin B_{12} associates with many enzymes, such as adenosylcobalamin-dependent isomerases, methylcobalamin-dependent methyltransferases, and dehalogenases.[4] Chronic feeding of a methyl-donor, vitamin B_{12}-deficient diet causes the spontaneous development of hepatocellular carcinoma.[5] Therefore, when the liver is injured, stored vitamin B_{12} leaks out into the blood, which causes a severe B_{12}-deficit in the liver, probably resulting in metabolic dysfunction. So far, it has been reported that vitamin B_{12} was effective for the liver protection against the acute liver injury.[6] However, there is no findings of the effect on chronic liver fibrosis. Therefore, we examined the effect of vitamin B_{12} on the fibrogenesis using chronically liver-injured mice.

Dimethylnitrosamine (DMN) is a potent hepatotoxin, carcinogen and mutagen. DMN induces liver fibrosis in a highly reproducible manner, first inducing a central hemorrhagic necrosis followed by the formation of septa and establishing micronodular cirrhosis after 3 weeks of treatment.[7] DMN-induced liver fibrosis in animals is a good and reproducible animal model for studying pathophysiological alterations associated with the development of liver fibrosis and cirrhosis in humans.[8,9] In this study, we found that the treatment of a chronic liver-injury model with vitamin B_{12} suppressed both liver inflammation and fibrosis.

MATERIALS AND METHODS

Animals BALB/c mice were purchased from SLC (Shimizu, Japan). The animals were housed in an air-conditioned room at 22 °C before the experiment. Hepatic injury in mice aged 6 weeks was elicited by the intraperitoneal administration of dimethylnitrosamine (DMN; Sigma, St. Louis, MO, U.S.A.) at 5 mg/kg body weight for the first 3 consecutive days of the week for 4 weeks. Vitamin B_{12} (Wako Pure Chemicals, Osaka, Japan) was administered intraperitoneally at 10 mg/kg body weight at the same time as DMN. After 4 weeks of treatment, the mice were anesthetized, and blood samples were taken from the orbital sinus. The animal experiments were conducted according to the ethical guidelines of the Osaka University Graduate School of Pharmaceutical Sciences.

Histological Analysis Liver specimens were fixed in 10% formaldehyde and embedded in paraffin. Sections were cut from the tissue blocks, mounted on slides, and stained with Elastica van Gieson (EG).

Assays Serum aspartate aminotransferase (AST) and alanine aminotransferase (ALT) levels were measured using an assay kit (Iatrozyme TA-Lq; Mitsubishi Kagaku Iatron Inc., Tokyo, Japan).

Reverse Transcription-Polymerase Chain Reaction (RT-PCR) The liver was excised and homogenized after removing the blood with phosphate-buffered saline. The total RNA was extracted from the liver homogenates using Sepasol-RNA I (Nacalai Tesque, Kyoto, Japan). The gene expression of α-smooth muscle actin (α-SMA) was analyzed by RT-PCR using the following primers: forward 5′-CAGGGAGTAATGGTTGGAAT-3′ and reverse 5′-CGTCGTATTCCTGTTTGCTGA-3′. Heat-shock protein 47 (HSP47) gene

* To whom correspondence should be addressed. e-mail: yagi@phs.osaka-u.ac.jp.

expression was analyzed using the following primers: forward 5′-CCATCGACAAGAACAGA-3′ and reverse 5′-TCATATTTCCCTTCCCCCCATC-3′. β-Actin gene expression was analyzed using the following primers: forward 5′-CATCCCCCAAAGTTCTAC-3′ and reverse 5′-CCAAAGC-CTTCATACATC-3′. RT was performed using 1 μg of total RNA sample with the BcaBEST RNA PCR kit (Takara, Kyoto, Japan). The PCR conditions were: 1) 94 °C for 1 min; 2) 30 cycles of 30 s at 94 °C, 30 s at 55 °C, and 1 min at 72 °C; 3) 72 °C for 5 min.

Statistics The data were analyzed for statistical significance by Student's *t*-test.

RESULTS AND DISCUSSION

We examined the hepatoprotective effect of vitamin B_{12} on DMN-induced liver injury in mice. As shown in Fig. 1, after 4 weeks of DMN treatment, the activities of blood AST and ALT increased 2.9- and 3.3-fold, respectively, compared with controls, and the intraperitoneal administration of vitamin B_{12} significantly decreased the activities of AST and ALT. These results suggest that vitamin B_{12} suppresses the hepatic inflammation caused by the DMN treatment.

We next examined the effect of vitamin B_{12} administration on liver injury and fibrogenesis (Fig. 2). Liver sections were prepared after 4 weeks of DMN treatment and examined by EG staining. EG staining showed the significant accumulation of collagen fibrils after DMN treatment. This accumulation was clearly lower in DMN-treated mice given vitamin B_{12}. DMN bioactivation is thought to occur through the liver mixed-fuction oxidases (cytochrome P450 2E1).[10] The end result is the formation of toxic intermediates such as hydroxyl radicals, reactive oxygen intermediates.[11] Therefore, vitamin B_{12} appears to protect liver from the oxidation stress caused by DMN.

To confirm the antifibrotic effect of vitamin B_{12}, we next examined the gene expression of α-SMA and HSP47, which are markers of fibrosis, using RT-PCR analysis. As shown in Fig. 3, marked upregulation of the expression of the α-SMA and HSP47 genes was observed in the DMN-injured liver compared with the control liver. Therefore, although the liver damage was not fatal, the long-term liver injury caused inflammation and resulted in fibrosis. Vitamin B_{12} significantly

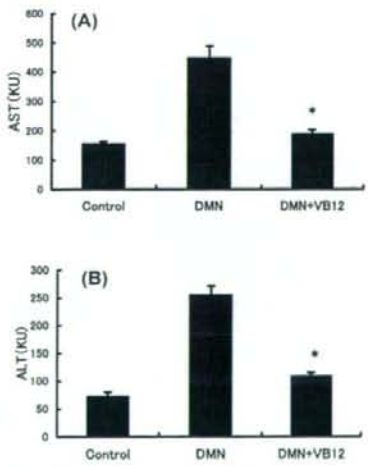

Fig. 1. Suppressive Effect of Vitamin B_{12} on Blood Transaminase Activities in DMN-Treated Mice

(A) AST, (B) ALT. DMN and vitamin B_{12} were injected intraperitoneally three times a week for 4 weeks. Values are the mean±S.D. ($n=3$ animals). *$p<0.05$, compared with DMN alone.

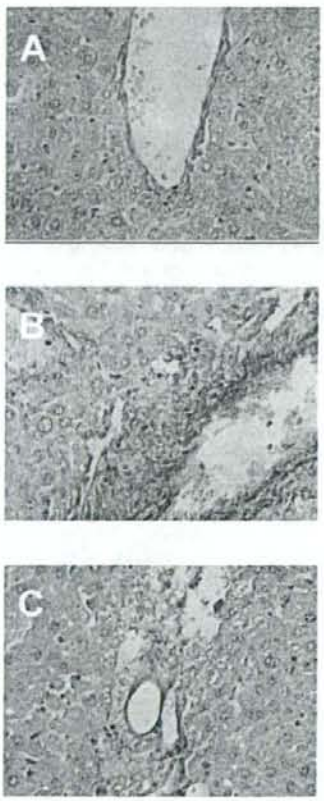

Fig. 2. Elastica van Gieson Staining for Collagen Fibrils

(A) Untreated control, (B) DMN treatment alone, (C) DMN and vitamin B_{12} treatment. Original magnification ×400.

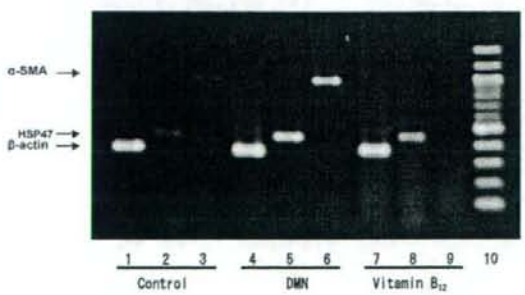

Fig. 3. RT-PCR Analysis of Gene Expression Related to Liver Fibrosis in DMN-Injured Mouse Liver

(Lanes 1, 4, 7) PCR products showing β-actin expression. (Lanes 2, 5, 8) HSP47 expression. (Lanes 3, 6, 9) α-SMA expression. Lane 10, molecular size markers.

suppressed the increased gene expression of both α-SMA and HSP47. Furthermore, in preliminary *in vitro* experiments, vitamin B_{12} protected rat primary hepatocytes from hepatotoxin-induced cell death. Therefore, vitamin B_{12} might suppress liver inflammation and the subsequent fibrogenesis by protecting hepatocytes from liver injury.

During liver injury, hepatic stellate cells (HSCs) are activated to transdifferentiate into myofibroblasts and overproduce extracellular matrix, which leads to fibrosis.[12] Oxidative stress stimulates the activation of HSCs, and substances with antioxidative activity, such as vitamin E,[13] glutathione,[14] and L-cysteine,[15] inhibit HSC activation, thus suppressing liver fibrosis. However, we have not found any antioxidative activity by vitamin B_{12} (data not shown). It has been reported that the activity of glutathione reductase was found to be significantly lower in B_{12}-deficient liver.[16] Recently, it was reported that the interaction between vitamin B_{12} and glutathione could protect against disease related to vitamin B_{12} deficiency.[17] Although vitamin B_{12} itself does not have radical scavenging ability, it might play an important role to maintain the sulfhydryl level under oxidative conditions. Vitamin B_{12} contains a cobalt complex and is widely used to describe compounds of the cobalamin group. It is possible that the cobalt complex of vitamin B_{12} is involved in the inhibition of liver inflammation and fibrogenesis, but further studies are necessary to clarify vitamin B_{12}'s mechanism of action.

We previously reported that $Zn(Mal)_2$ suppresses cytotoxin-induced apoptotic and necrotic cell death in isolated hepatocytes.[18] This zinc complex has free-radical scavenging activity. Several manganic porphyrins mimicked superoxide dismutase and had protective effect against oxidative stress.[19,20] Finally, here we found that the increase in α-SMA and HSP47 gene expression caused by DMN treatment was suppressed by vitamin B_{12}. Thus, a variety of metal complexes seem to have therapeutic potential.

In conclusion, we found that vitamin B_{12} is potent a hepatoprotective agent. This report is the first to demonstrate the hepatoprotective effect of vitamin B_{12} on liver fibrosis.

REFERENCES

1) Abeles R. H., Dolphin H., *Acc. Chem. Res.*, **9**, 114—120 (1976).
2) Areekul S., Hitanant S., Panatampon P., Chantachum Y., *Southeast Asian J. Trop Med. Public Health*, **8**, 519—524 (1977).
3) Ermens A. A., Vlasveld L. T., Lindemans J., *Clin. Biochem.*, **36**, 585—590 (2003).
4) Banerjee R., Ragsdale S. W., *Annu. Rev. Biochem.*, **72**, 209—247 (2003).
5) Asada K., Kotake Y., Asada R., Saunders D., Broyles R. H., Towner R. A., Fukui H., Floyd R. A., *J. Biomed. Biotechnol.*, **2006**, 17142 (2006).
6) Kasbekar D. K., Lavate W. V., Rege D. V., Sreenivasan A., *Biochem. J.*, **72**, 384—389 (1959).
7) Jezequel A. M., Mancini R., Rinaldesi M. L., Macarri G., Venturini C., Orlandi F., *J. Hepatol.*, **5**, 174—181 (1987).
8) Jezequel A. M., Mancini R., Rinaldesi M. L., Ballardini G., Fallani M., Bianchi F., Orlandi F., *J. Hepatol.*, **8**, 42—52 (1989).
9) Jin Y. L., Enzan H., Kuroda N., Hayashi Y., Toi M., Miyazaki E., Hamauzu T., Hiroi M., Guo L. M., Shen Z. S., Saibara T., *Med. Mol. Morphol.*, **39**, 33—43 (2006).
10) Dicker E., Cederbaum A. I., *Alcohol. Clin. Exp. Res.*, **15**, 1072—1076 (1991).
11) Montesano R., Bartsch H., *Mutat. Res.*, **32**, 179—228 (1976).
12) Friedman S. L., Roll F. J., Boyles J., Arenson D. M., Bissell D. M., *J. Biol. Chem.*, **264**, 10756—10762 (1989).
13) Houglum K., Venkataramani A., Lyche K., Chojkier M., *Gastroenterology*, **113**, 1069—1073 (1997).
14) Maher J. J., Saito J. M., Neuschwander-Tetri B. A., *Biochem. Pharmacol.*, **53**, 637—641 (1997).
15) Horie T., Sakaida I., Yokoya F., Nakajo M., Sonaka I., Okita K., *Biochem. Biophys. Res. Commun.*, **305**, 94—100 (2003).
16) Biswas D. K., Johnson B. C., *Arch. Biochem. Biophys.*, **104**, 375—380 (1964).
17) Watson W. P., Munter T., Golding B. T., *Chem. Res. Toxicol.*, **17**, 1562—1567 (2004).
18) Kawase M., Kagaya N., Akamatsu S., Kamiyoshi A., Muto S., Tagawa Y., Yagi K., *Exp. Anim.*, **53**, 1—9 (2004).
19) Faulkner K. M., Liochev S. I., Fridovich I., *J. Biol. Chem.*, **269**, 23471—23476 (1994).
20) Szabo C., Day B. J., Salzman A. L., *FEBS Lett.*, **381**, 82—86 (1996).

THE JOURNAL OF BIOLOGICAL CHEMISTRY VOL. 283, NO. 2, pp. 998–1007, January 11, 2008

Creation and X-ray Structure Analysis of the Tumor Necrosis Factor Receptor-1-selective Mutant of a Tumor Necrosis Factor-α Antagonist*

Received for publication, September 21, 2007, and in revised form, November 2, 2007 Published, JBC Papers in Press, November 14, 2007, DOI 10.1074/jbc.M707933200

Hiroko Shibata,[a,b] Yasuo Yoshioka,[a,c] Akiko Ohkawa,[a] Kyoko Minowa,[a,d] Yohei Mukai,[a,e] Yasuhiro Abe,[a,e] Madoka Taniai,[f] Tetsuya Nomura,[a,e] Hiroyuki Kayamuro,[a,e] Hiromi Nabeshi,[a,e] Toshiki Sugita,[a,e] Sunao Imai,[a,e] Kazuya Nagano,[a,e] Tomoaki Yoshikawa,[a] Takuya Fujita,[d] Shinsaku Nakagawa,[c,e] Akira Yamamoto,[d] Tsunetaka Ohta,[f] Takao Hayakawa,[b] Tadanori Mayumi,[g] Peter Vandenabeele,[h] Bharat B. Aggarwal,[i] Teruya Nakamura,[j] Yuriko Yamagata,[j] Shin-ichi Tsunoda,[a,c] Haruhiko Kamada,[a,c1] and Yasuo Tsutsumi[a,c,e]

From the [a]National Institute of Biomedical Innovation, 7-6-8 Saito-Asagi, Ibaraki, Osaka 567-0085, Japan, [b]National Institute of Health Science, 1-18-1 Kamiyoga, Setagaya-ku, Tokyo 158-8501, Japan, [c]Center for Advanced Medical Engineering and Informatics, Osaka University, 1-6 Yamadaoka, Suita, Osaka 565-0871, Japan, [d]Kyoto Pharmaceutical University, Misasagi-Nakauchicho 5, Yamashina-ku, Kyoto 607-8414, Japan, [e]Graduate School of Pharmaceutical Sciences, Osaka University, 1-6 Yamadaoka, Suita, Osaka 565-0871, Japan, [f]Hayashibara Biochemical Laboratories, Inc., 1-2-3 Shimoishii, Okayama 702-8006, Japan, [g]Graduate School of Pharmaceutical Sciences, Kobe Gakuin University, 518 Arise, Igawadani, Nishi-ku, Kobe 651-2180, Japan, the [h]Department of Molecular Biomedical Research, Flanders Institute for Biotechnology and the Department of Molecular Biology, Ghent University, B-9052 Ghent, Belgium, the [i]Department of Experimental Therapeutics, University of Texas M. D. Anderson Cancer Center, Houston, Texas 77030, and [j]Faculty of Medical and Pharmaceutical Sciences, Kumamoto University, 5-1 Ooehonmachi, Kumamoto 862-0973, Japan

Tumor necrosis factor-α (TNF) induces inflammatory response predominantly through the TNF receptor-1 (TNFR1). Thus, blocking the binding of TNF to TNFR1 is an important strategy for the treatment of many inflammatory diseases, such as hepatitis and rheumatoid arthritis. In this study, we identified a TNFR1-selective antagonistic mutant TNF from a phage library displaying structural human TNF variants in which each one of the six amino acid residues at the receptor-binding site (amino acids at positions 84–89) was replaced with other amino acids. Consequently, a TNFR1-selective antagonistic mutant TNF (R1antTNF), containing mutations A84S, V85T, S86T, Y87H, Q88N, and T89Q, was isolated from the library. The R1antTNF did not activate TNFR1-mediated responses, although its affinity for the TNFR1 was almost similar to that of the human wild-type TNF (wtTNF). Additionally, the R1antTNF neutralized the TNFR1-mediated bioactivity of wtTNF without influencing its TNFR2-mediated bioactivity and inhibited hepatic injury in an experimental hepatitis model. To understand the mechanism underlying the antagonistic activity of R1antTNF, we analyzed this mutant using the surface plasmon resonance spectroscopy and x-ray crystallography. Kinetic association/dissociation parameters of the R1antTNF were higher than those of the wtTNF, indicating very fast bond dissociation. Furthermore, x-ray crystallographic analysis of R1antTNF suggested that the mutation Y87H changed the binding mode from the hydrophobic to the electrostatic interaction, which may be one of the reasons why R1antTNF behaved as an antagonist. Our studies demonstrate the feasibility of generating TNF receptor subtype-specific antagonist by extensive substitution of amino acids of the wild-type ligand protein.

Tumor necrosis factor (TNF)[2] is a major inflammatory cytokine that, like the other members of the TNF superfamily of ligands, plays a central role in host defense and inflammation (1). Elevated serum levels of TNF correlate with the severity and progression of the inflammatory diseases such as rheumatoid arthritis, inflammatory bowel disease, septic shock, multiple sclerosis, and hepatitis (2–4). So far, anti-TNF antibodies and soluble TNFRs, which interfere with the activity of TNF, have been used to treat various inflammatory diseases (5, 6). However, these therapies can cause serious side effects, such as bacterial and virus infection, lymphoma development, and lupus inflammatory disease (7–10), because they also inhibit the TNF-

* This work was supported in part by Grants-in-aid for Scientific Research 18015055, 18659047, and 7689008 from the Ministry of Education, Culture, Sports, Science and Technology of Japan and Japan Society for the Promotion of Science, by a Health Labor Sciences research grant from the Ministry of Health, Labor and Welfare of Japan, by Health Sciences research grants for research on health sciences focusing on drug innovation from the Japan Health Sciences Foundation, and in part by Japan Society for the Promotion of Science Research Fellowships for Young Scientists 02872, 08841, 09131. The costs of publication of this article were defrayed in part by the payment of page charges. This article must therefore be hereby marked "*advertisement*" in accordance with 18 U.S.C. Section 1734 solely to indicate this fact.

The atomic coordinates and structure factors (code 2E7A) have been deposited in the Protein Data Bank, Research Collaboratory for Structural Bioinformatics, Rutgers University, New Brunswick, NJ (http://www.rcsb.org/).

[1] To whom correspondence should be addressed: Laboratory of Pharmaceutical Proteomics, National Institute of Biomedical Innovation, 7-6-8 Saito-Asagi, Ibaraki, Osaka 567-0085, Japan. Fax: 81-72-641-9817; E-mail: kamada@nibio.go.jp.

[2] The abbreviations used are: TNF, tumor necrosis factor α; TNFR, TNF receptor; PDB, Protein Data Bank; PBS, phosphate-buffered saline; RT, reverse transcription; HUVEC, human umbilical vein endothelial cells; ELISA, enzyme-linked immunosorbent assay; GM-CSF, granulocyte-macrophage colony-stimulating factor; TES, 2-{[2-hydroxy-1,1-bis(hydroxymethyl)ethyl]amino}ethanesulfonic acid; EAE, experimental autoimmune encephalomyelitis; ALT, alanine aminotransferase; h, human; m, mouse; mut, mutant.

dependent host defense function of the patients. TNF blockade by administering these agents into patients with multiple sclerosis was also shown to aggravate their symptoms (11). Therefore, to overcome these problems, development of a new therapeutic strategy is highly desirable.

TNF binds to two receptor subtypes, p55 TNF receptor (TNFR1) and p75 TNF receptor (TNFR2), to exert its biological functions (12). Thus, functional analyses of the TNF receptors were carried out to explore a new therapeutic strategy. Previous studies using animal models of diseases such as arthritis and hepatitis demonstrated the predominant role of TNFR1 in the pathogenesis and exacerbation of inflammation (13, 14). In the experimental autoimmune encephalomyelitis model (EAE), which is widely used as an animal model of multiple sclerosis, the symptoms exacerbated significantly in the TNF knock-out mice compared with that in the wild-type mice (15). Another study indicates that the TNF has a dual role on the EAE model, an inflammatory and immunosuppressive effect, and although the immunosuppressive effect does not require the TNFR1, it is essential for the acute phase inflammation of EAE (16). On the other hand, although the TNFR1 is believed to be important for the defense mechanism against mycobacterium, the membrane-bound TNF, the prime activating ligand of TNFR2, was reported to be sufficient to control the mycobacterial infection (17, 18). Moreover, TNFR2 was shown to be crucial for the proliferation, activation, and antigen presentation of the T-cells, which are essential in the cell-mediated immune response against bacteria and virus (19–21). Therefore, blocking the TNFR1-mediated signal transduction emerged as a potential therapeutic strategy with low side effects for the inflammatory diseases.

From these perspectives, attempts were made to develop drugs targeted to TNFR1. Along with the progress of antibody engineering, attempts were made to develop an anti-TNFR1 antibody with antagonistic activity. But the desired antibody could not be created, because the anti-TNFR1 antibodies recognizing the TNF-binding site on TNFR1 acted like a TNFR1 agonist and not an antagonist (22). Attempts to design a low molecular weight TNFR1 antagonist based on the three-dimensional structural information of the TNFR1 was also not successful in identifying an antagonist that would selectively inhibit the TNF/TNFR1 interaction and would have sufficient therapeutic effect (23, 24). In this respect, we previously 1) constructed two phage libraries displaying the structural TNF variants in which six amino acid residues (amino acids 29, 31, 32, 145–147, library I; amino acids 84–89, library II) in the predicted receptor binding sites were replaced with other amino acid, 2) and we successfully identified the TNFR1-selective mutant with great biological activity from the library I.[3] In the screening process, mutants with high affinity for the TNFR1 and great TNFR1 selectivity were found from library II, although their biological activities were very weak.[3] The strategy described here could comprehensively assess the affinities and bioactivities of TNF variants, thus enabling the high-throughput screening of TNFR1-selective antagonists, which have no biological activity but high TNFR1 affinity. In this study, we analyzed the biological activity and TNFR1 affinity of 500 TNF variants, which were concentrated by panning against the TNFR1, and we subsequently isolated a novel TNFR1-selective antagonistic mutant TNF (R1antTNF). R1antTNF showed exclusive TNFR1 selectivity, and it efficiently inhibited wide varieties of TNFR1-mediated effects of the wild-type TNF *in vitro* and *in vivo*. Additionally, we used surface plasmon resonance and x-ray structural analyses to elucidate the underlying cause for the antagonist activity of R1antTNF.

[3] Y. Abe, H. Shibata, K. T. Nomura, K. Minowa, H. Kamada, S. Tsunoda, Y. Tsutsumi, unpublished data.

EXPERIMENTAL PROCEDURES

Cell Culture—L-M cells (a mouse fibroblast cell line) were provided by Mochida Pharmaceutical Co. Ltd. (Tokyo, Japan) and were maintained in minimum Eagle's medium (Sigma) supplemented with 1% fetal bovine serum and 1% antibiotic mixture (penicillin 10,000 units/ml, streptomycin 10 mg/ml, and amphotericin B 25 μg/ml) (Nacalai Tesque, Kyoto, Japan). HEp-2 cells (a human fibroblast cell line) were provided by Cell Resource Center for Biomedical Research (Tohoku University, Sendai, Japan) and were maintained in RPMI 1640 medium (Sigma) supplemented with 10% fetal bovine serum and 1% antibiotic mixture (Nacalai Tesque). PC60-R1 and PC60-R2 cells (a mouse-rat fusion hybridoma consisting of human TNFR1- or TNFR2-transfected PC60 cells) were established as described previously (25) and maintained in RPMI 1640 medium supplemented with 10% fetal bovine serum, 1 mM sodium pyruvate, 5×10^{-5} M 2-mercaptoethanol, 3 μg/ml puromycin (Wako Pure Chemical Industries, Osaka, Japan), and 1% antibiotic mixture.

Cytokines, Receptors, and Antibodies—Recombinant human TNFR1 or TNFR2 Fc chimera, biotinylated anti-human TNF polyclonal antibody, and horseradish peroxidase-conjugated horseradish peroxidase were purchased from R & D Systems (Minneapolis, MN). Recombinant human or mouse TNF and IL-1β were purchased from PeproTech (Rocky Hill, NJ). The recombinant human TNF used for the *in vivo* hepatitis examination and the recombinant wtTNF-FLAG (a FLAG tag fusion protein of human TNF) were purified in our laboratory. We confirmed that the bioactivity of each TNF was equal to that of commercially available recombinant human TNF. Anti-FLAG M2 antibody was purchased from Sigma. Goat anti-human IgG antibody was purchased from Cappel (West Chester, PA). Anti-human Fas IgM was purchased from MBL (Nagoya, Japan).

Selection of Phage Displaying Structural TNF Variants (Panning)—Human TNFR1 Fc chimera was diluted to 50 μg/ml in 10 mM sodium acetate buffer, pH 4.5, and immobilized to a CM3 sensor chip using an amine coupling kit (BIAcore®, Uppsala, Sweden), which resulted in an increase of 4,000–6,000 resonance units. The phage library (1×10^{11} colony-forming units/100 μl) was injected at the flow rate of 3 μl/min over the sensor chip. After injection, the sensor chip was washed using the rinse command. Elution was carried out using 20 μl of 10 mM glycine HCl. The eluted phages were neutralized with 1 M Tris-HCl, pH 6.9. *Escherichia coli* (TG1) was infected with the eluted phages for amplification. These steps were performed twice. After the second round of selection, the phage mixture was used to infect *E. coli* and plated on LB agar/ampicillin

plates. Five hundred individual colonies of *E. coli* infected with phage clones were individually picked from the LB agar plates, and each colony was grown in 2-YT medium with ampicillin (100 μg/ml) and glucose (2% w/v) at 37 °C until the A_{600} of the culture medium reached 0.4. Each culture was centrifuged; the supernatants were removed, and fresh 2-YT media with ampicillin (100 μg/ml) was added to each *E. coli* pellet. After incubation for 6 h at 37 °C, supernatants were collected and used to measure cytotoxicity in human HEp-2 cells (26, 27) and to determine the affinity for TNFR1 by ELISA (28). To measure cytotoxicity, HEp-2 cells were cultured in 96-well plates with 10% *E. coli* supernatant and 100 μg/ml cycloheximide for 18 h at 4×10^4 cells/well, and cytotoxicity was assessed by methylene blue assay as described previously (26). To determine the affinity for TNFR1 by ELISA, wells of the immune assay plates were first coated with the goat anti-human IgG antibody and then incubated with the recombinant human TNFR1 Fc chimera (0.2 μg/ml). After blocking, 2-fold diluted *E. coli* supernatant was added into each well, and the plates were incubated for 2 h at 37 °C. To each well, 200 ng/ml biotinylated anti-human TNF polyclonal antibody was added, and the plates were further incubated for 1 h at 37 °C. Wells were washed and then incubated with 1000-fold diluted avidin-horseradish peroxidase. Next, wells were washed; TMB peroxidase substrate (MOSS, Inc. Pasadena, MD) was added to each well, and the absorbance was read at 450/650 nm using a micro-plate reader.

Expression and Purification of mutTNFs—Protocol for the expression and purification of recombinant proteins was described previously (29). Briefly, mutTNFs were overexpressed in *E. coli* BL21(DE3). Expressed mutTNFs were recovered from the inclusion body, which were washed with 2.5% Triton X-100 and 0.5 M NaCl in TES buffer, and solubilized in 6 M guanidine HCl, 0.1 M Tris-HCl, pH 8.0, and 2 mM EDTA. The solubilized protein was reduced with 10 mg/ml dithioerythritol for 4 h at room temperature and then refolded by 100-fold dilution in a refolding buffer (100 mM Tris-HCl, 2 mM EDTA, 0.5 M arginine, and oxidized glutathione (551 mg/liter)). After dialyzing against 20 mM Tris-HCl, pH 7.4, containing 100 mM urea, the active trimeric proteins were purified by Q-Sepharose and Mono Q chromatography. An additional size-exclusion chromatography (Superose 12, GE Healthcare) was performed to further purify each protein. Endotoxin levels in the purified mutTNF were determined to be <300 pg/mg.

Cytotoxicity Assay—For the cytotoxicity assay, mouse L-M cells were cultured in the 96-well plates (1×10^4 cells/well) in the presence of serially diluted mouse wtTNF or mutTNFs. For the neutralization assay, cells were cultured in the presence of a constant concentration of the mouse wtTNF (5 ng/ml) and a serial dilution of the mutTNF. After incubation for 48 h, cell survival was determined by methylene blue assay as described previously (26). Jurkat cells were incubated in 96-well plates (1×10^4 cells/well) with 0.2 ng/ml anti-human Fas IgM and serially diluted R1antTNF for 24 h, and cytotoxicity was assessed using the 3-(4,5-dimethylthiazol-2-yl)-2,5-diphenyltetrazolium bromide assay.

Competitive ELISA—Inhibition of wtTNF binding to the hTNFR1 and hTNFR2 by R1antTNF was measured by ELISA as reported previously (28). The wtTNF-FLAG, a FLAG tag fusion protein of human TNF, was used as a marker protein. Briefly, the immune assay plates were coated with the goat anti-human IgG antibody and incubated with either the human TNFR1 or the human TNFR2 (0.2 μg/ml). After blocking, premixed wtTNF-FLAG (100 ng/ml) and various concentrations of R1antTNF were added to the plates. After 2 h of incubation at room temperature, the wells were washed, and the biotinylated anti-FLAG M2 antibody (0.5 μg/ml) was added to each well and then incubated for an additional period of 2 h at room temperature. Wells were washed and then incubated with the horseradish peroxidase-coupled streptavidin for 30 min at room temperature. The remaining bound wtTNF-FLAG was quantified as described above.

PC60 Assay—PC60-R1 and PC60-R2 cells were cultured at 5×10^4 cells/well with IL-1β (2 ng/ml). To evaluate the inhibitory activity, serially diluted R1antTNF and human wtTNF (200 ng/ml for PC60-R1 and 40 ng/ml for PC60-R2) were added to each cell type. After 24 h of incubation, the amount of rat GM-CSF produced was quantified by ELISA according to the manufacturer's protocol (R & D Systems).

Caspase-3/7 and NF-κB Activities—To measure the caspase-3/7 activity, the L-M cells were incubated with the human wtTNF (60 ng/ml) and R1antTNF for 8 h, and then an equal volume of the Caspase-Glo 3/7 Assay reagent (Promega Japan, Tokyo, Japan) was added to the cells. The cells were further incubated for 1 h, and luminescence was then measured using a plate reader (ALVO series, PerkinElmer Life Sciences). To measure the NF-κB activity, nuclear proteins were collected from the L-M cells stimulated with the human wtTNF (5 ng/ml) and R1antTNF for 1 h, and the activity of the NF-κB p65 in the treated cells was determined using the TransAM NF-κB p65 kit (Active Motif, Carlsbad, CA). Nuclear protein extract (1 μg) was added to an oligonucleotide-coated plate and was visualized using an anti-NF-κB p65 antibody.

RT-PCR Analysis—Total RNA was extracted from the human wtTNF and R1antTNF-stimulated HUVEC using an RNeasy mini kit (Qiagen, Valencia, CA). First-strand cDNA was synthesized from 1 μg of total RNA by using an oligo(dT_{12-18}) primer and SuperScript III reverse transcriptase (Invitrogen). Real time quantitative RT-PCR was performed using the TaqMan assay, and the PCR amplifications were carried out using an ABI 7000 thermocycler (Applied Biosystems, Foster City, CA). cDNA samples were added into a PCR master mix containing the Platinum qPCR super mix (Invitrogen) and primer/fluorescent probe sets (TaqMan Gene Expression Assays, Applied Biosystems) for the human β-actin, E-selectin, and ICAM-1 in 96-well PCR plates. Conditions for PCR were 2 min at 50 °C, 2 min at 95 °C, 45 cycles of denaturation at 95 °C for 15 s, and annealing/extension step at 60 °C for 5 s. The threshold cycle (*CT*) during the exponential phase of amplification was determined using the ABI Prism® 7000 SDS software.

Induction of Lethal Hepatitis—BALB/c mice (6-week-old females) were purchased from CLEA Japan (Tokyo, Japan). All experimental protocols for animal studies were in accordance with "Principles of Laboratory Animal Care" (National Institutes of Health) and our institutional guidelines. All reagents were prepared in pyrogen-free PBS. Control mice were injected

intravenously with 200 μl of the mixture, 100 μl of PBS, 50 μl of 20 μg/ml wtTNF, and 50 μl of 400 mg/ml GalN. Experimental mice were injected intravenously with 200 μl of the mixture, 100 μl of R1antTNF (2.7, 0.3, or 0.1 mg/ml), 50 μl of 20 μg/ml wtTNF, and 50 μl of 400 mg/ml GalN. In preliminary experiments, serum ALT levels began to increase at 6 h and were maximal 9 h after the administration of TNF/GalN. The dose used was lethal in 80–100% of mice. Blood samples were obtained from the orbital plexus under light ether anesthesia 9 h after the challenge. The serum ALT concentration was measured using a colorimetric assay kit from Wako Pure Chemical (Osaka, Japan).

Surface Plasmon Resonance Assay (BIAcore® Assay)—The binding kinetics of the wtTNF and R1antTNF were analyzed by the surface plasmon resonance (BIAcore®) technique. TNFRs were immobilized onto a CM5 sensor chip, which resulted in an increase of 3,000–3,500 resonance units. During the association phase, R1antTNF or wtTNF, diluted in running buffer (HBS-EP) at 26.1 nM, 8.7 nM or 2.9 nM, was allowed to pass over the immobilized TNFRs at a flow rate of 20 μl/min. During the dissociation phase, HBS-EP buffer was applied to the sensor chip at a flow rate of 20 μl/min. The data were analyzed globally with the BIAevaluation 3.0 software (BIAcore®) using a 1:1 binding model.

X-ray Crystallography—Purified R1antTNF was concentrated to 10 mg/ml in 20 mM Tris-HCl, pH 7.4. Initial screening using Hampton Crystal screen 1, 2 and Index kit was performed by the vapor-diffusion method with hanging drops (1 + 1 μl) at 20 °C. After optimization of crystallization conditions, orthorhombic crystals ($0.2 \times 0.2 \times 0.4$ mm^3) were obtained with 0.05 M HEPES, pH 7.5, 1.5% w/v 1,2,3-heptanetriol, and 12.5% PEG 3350. Crystals were frozen in a reservoir solution containing 20% glycerol as a cryoprotectant. X-ray diffraction data to 1.8 Å resolution were collected at the BL41XU, SPring-8 synchrotron, Harima, Japan, under flash-cooling to 100 K to reduce the effects of radiation damage. Data reduction was carried out using the DENZO and SCALEPACK. Molecular replacement was performed by using the Molrep program in ccp4i (30) using a crystal structure of the wtTNF (1TNF) (31) as a model. Cycles of manual rebuilding using O (32) and refinement using CNS (33) led to a refined structure. Final model validation was performed using the Procheck program in ccp4i (30). The model complexes of TNF-TNFR1 and R1antTNF-TNFR1 were constructed based on the crystal structure of the LT-α-TNFR1 complex (31) by using the superpose program in ccp4i.

RESULTS

Selection of TNFR1-selective mutTNF Antagonists—We previously constructed a phage library that displays structural variants of the human TNF in which random amino acid sequences replace the 6 residues (amino acids 84–89) that have been predicted to be in the TNF receptor-binding site from the crystal structure of the LT-α-TNFR1 complex (31). We confirmed that the phage library consisted of 1×10^7 independent recombinant clones. To isolate a TNFR1-selective mutant TNF (mutTNF) antagonist, the phage library was subjected to two rounds of panning against the human TNFR1 (hTNFR1) using the BIAcore® biosensor, and recovered clones were assessed for

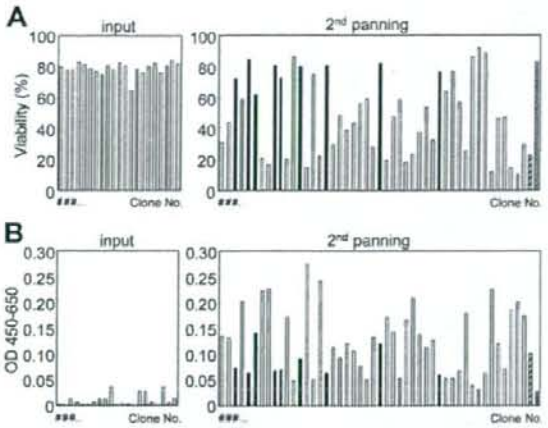

FIGURE 1. **Screening of TNFR-selective mutTNFs with no bioactivity.** Selected phage clones from the phage library were used to infect *E. coli* in a 96-well plate, and the supernatant from each infected *E. coli* was assessed to determine the bioactivity (*A*) and binding affinity (*B*) of each mutTNF. *A*, Hep-2 cells were incubated with the *E. coli* supernatant for 18 h, and cell viability was measured using the methylene blue assay. *B*, each *E. coli* supernatant was applied to the TNFR1-immobilized plate, and binding of the mutTNF to the TNFR1 was detected using the biotinylated polyclonal anti-TNF antibody. ■, mutTNF clones binding specifically to TNFR1; ▨, wtTNF; ▤, negative control.

TABLE 1
Nucleotide and amino acid sequences of 10 candidate TNFR1-selective mutTNF antagonists, which had high affinity for TNFR1 and no TNFR1 bioactivity

Clone	Position					
	Ala-84	Val-85	Ser-86	Tyr-87	Gln-88	Thr-89
T1	G(GGC)	H(CAC)	L(TCC)	Y(TAC)	T(ACG)	T(AAC)
T2	S(AGC)	T(ACC)	T(ACC)	H(CAC)	N(AAC)	Q(CAG)
T3	T(ACC)	S(AGC)	V(GTC)	Y(TAC)	P(CCC)	H(CAC)
T4	T(ACC)	N(AAC)	I(ATC)	Y(TAC)	S(AGC)	N(AAC)
T5	N(AAC)	G(GGC)	A(GCG)	Y(TAC)	E(GAG)	T(ACG)
T6	G(GGC)	G(GGC)	P(CCG)	Y(TAC)	Q(CAG)	R(CGG)
T7	S(AGC)	P(CCG)	R(AGG)	V(GTC)	S(TCC)	G(GGC)
T8	T(ACC)	P(CCC)	A(GCC)	I(ATC)	N(AAC)	R(CGG)
T9	A(GCG)	P(CCC)	G(GGC)	Y(TAC)	S(TCC)	H(CAC)
T10	S(TCC)	P(CCC)	Q(CAG)	Y(TAC)	S(AGC)	V(GTC)

TNFR1-mediated cytotoxicity and affinity for TNFR1. Although the number of phage clones that had strong cytotoxicity increased after the second panning, phage clones having almost no cytotoxicity but significant affinity for TNFR1 were also recognized (Fig. 1). Eventually, we identified 10 mutTNF candidates as the TNFR1-selective antagonists (Table 1), and we further investigated the properties of these 10 potential antagonists. All 10 mutTNFs were recombinantly expressed in *E. coli*, out of which we could only purify nine mutTNFs (T1–T4, T6–T10); for some unknown reason, we were unable to purify the mutTNF-T5. All nine purified mutTNFs displayed a molecular mass of 17 kDa by gel electrophoresis and gel filtration analyses and formed homotrimeric complexes in the same manner as the wtTNF (data not shown). We measured the bioactivities and antagonistic activities of nine mutTNFs on the mouse TNFR1 (mTNFR1) using the L-M cells, a cell line derived from the L929 cells, and the results are shown in Fig. 2. The mutTNF-T2 showed the lowest biological activity even when tested at high concentrations (Fig. 2*A*). Both mutTNF-T2 and mutTNF-T7 inhibited the wtTNF-induced cytotoxicity

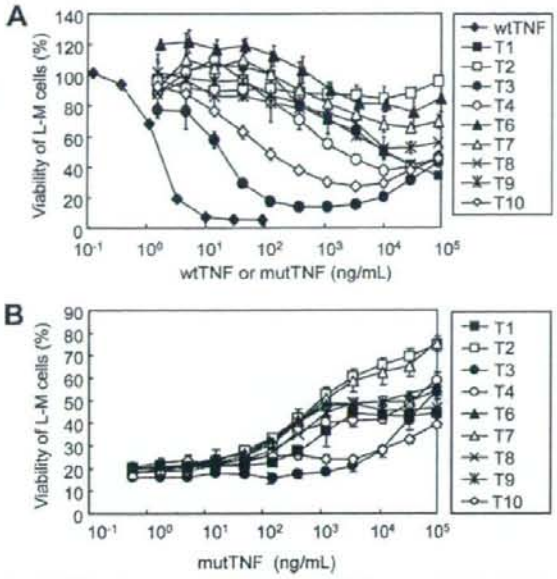

FIGURE 2. **Bioactivities and antagonistic activities of candidate TNFR1-selective mutTNFs.** *A*, diluted mutTNFs were added to the L-M cells and incubated for 48 h at 37 °C. After incubation, cell viability was measured using the methylene blue assay. *B*, indicated dilutions of a given mutTNF and a constant concentration of mouse TNF (5 ng/ml) were mixed and added to the L-M cells. Cell viability was measured as described above, and the antagonistic activity was assessed as described under "Experimental Procedures." Each data point represents the mean ± S.D.

TABLE 2

Dissociation constants of the mutTNFs determined from the SPR analysis of the interactions between the mutTNFs and the hTNFR1 or hTNFR2

Clone	TNFR1 K_D	TNFR2 K_D	TNFR1 selectivity
	nM	nM	
wtTNF	1.4	2.1	1.0
T1	5.0	28.1	3.7
T2	3.5	92,900.0	17,677.4
T3	1.2	4.6	2.6
T4	5.0	26.9	3.5
T6	7.6	2.3	0.2
T7	2.3	12.9	3.7
T8	2.6	1230.0	308.8
T9	6.8	8.4	0.8
T10	5.1	8.8	1.1

most efficiently (Fig. 2*B*). Additionally, the TNF receptor selectivity of the nine mutants was measured using the BIAcore® biosensor technique. Both mutTNF-T2 and mutTNF-T8 showed superior TNFR1 selectivity as compared with the other mutants (Table 2). Based on these results, mutTNF-T2 was chosen for further analysis and renamed as R1antTNF; this mutant displayed the highest selectivity for TNFR1 binding and possessed the lowest biological activity and highest antagonistic activity on mTNFR1.

Inhibition of TNFR1-mediated Intracellular Signaling and Expression of Adhesion Molecule by R1antTNF—Activation of TNFR1 by TNF leads to the recruitment of the adaptor protein TRADD to its cytoplasmic death domain and induction of apoptosis because of the activation of caspase-8/10 and caspase-3/7 (34). If R1antTNF inhibited the wtTNF-mediated cytotoxicity

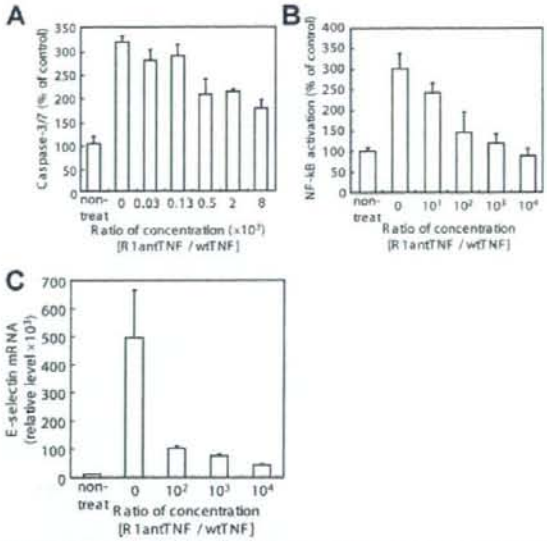

FIGURE 3. **R1antTNF-mediated inhibition of signal transduction and expression of adhesion molecule.** Activation of caspase-3/7 (*A*) and NF-κB (*B*) induced by the human wtTNF (60 and 5 ng/ml, respectively) in L-M cells was measured as described under "Experimental Procedures." Incubation times for the caspase-3/7 was 8 h and that for the NF-κB was 1 h. *C*, to measure the E-selectin expression, indicated amounts of R1antTNF were mixed with the human wtTNF (10 ng/ml), and the mixture was added to the HUVEC and incubated for 3 h. Total RNAs were prepared from these cells and were used for the RT-PCR analysis. Each data point represents the mean ± S.D.

in L-M cells by blocking the binding of wtTNF to TNFR1, R1antTNF could also inhibit this activation of caspase cascade. Thus, we investigated the inhibitory activity of R1antTNF on the wtTNF-induced activation of caspase-3/7. Indeed R1antTNF significantly inhibited the caspase-3/7 activation induced by the wtTNF in L-M cells in a dose-dependent manner (Fig. 3*A*). TNFR1 signaling also activates the transcription factor NF-κB, leading to the activation of inflammatory and anti-apoptotic genes (34). We found that the wtTNF-mediated NF-κB activation in mouse L-M cells was completely blocked by the addition of R1antTNF (Fig. 3*B*). NF-κB activated by the TNF/TNFR1 interaction regulates several cell adhesion molecules in the endothelial cells, such as E-selectin, ICAM-1, and VCAM-1 (35). Therefore, we assessed the inhibitory activity of R1antTNF on the wtTNF-induced expression of cell adhesion molecules in HUVEC cells. We found that the R1antTNF suppressed the expression of the E-selectin gene (Fig. 3*C*). These results suggested that R1antTNF inhibited the function of wtTNF by blocking the wtTNF-induced signal transduction.

TNFR1-selective Antagonistic Activity of R1antTNF—To determine the potency of the TNFR1-selective antagonistic activity, we used competitive ELISA to investigate whether the R1antTNF would inhibit only the binding of the wtTNF to hTNFR1. R1antTNF inhibited the binding of wtTNF to hTNFR1 in a dose-dependent manner just like the wtTNF did, but it did not affect the binding of wtTNF to hTNFR2 (Fig. 4, *A* and *B*). This result correlates to the results obtained using the BIAcore technique. To confirm that this antagonistic activity of R1antTNF was receptor-selective, a competitive bioassay was

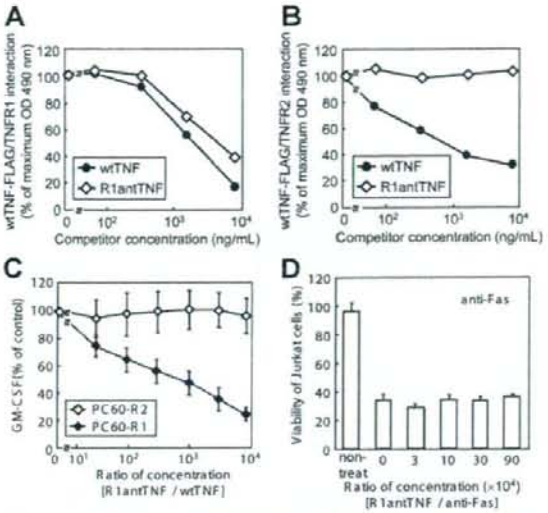

FIGURE 4. **TNFR1-selective antagonistic properties of R1antTNF.** Different concentrations of wtTNF and R1antTNF were premixed with a fixed concentration of wtTNF-FLAG and were added to the hTNFR1-coated (*A*) or hTNFR2-coated plates (*B*). Binding of wtTNF-FLAG was determined as described under "Experimental Procedures." *C*, to determine the receptor-type contribution to bioactivity, serially diluted R1antTNF was mixed with the human wtTNF (PC60-R1, 200 ng/ml; PC60-R2, 40 ng/ml), and added to the PC60-Rs cells. After 24 h, production of the rat GM-CSF was measured by ELISA as described under "Experimental Procedures." ♦, PC60-R1; 224 , PC60-R2. *D*, Jurkat cells were incubated with the anti-human Fas IgM (0.2 ng/ml) and indicated dilutions of R1antTNF for 24 h, and cytotoxicity was assessed using the 3-(4,5-dimethylthiazol-2-yl)-2,5-diphenyltetrazolium bromide assay.

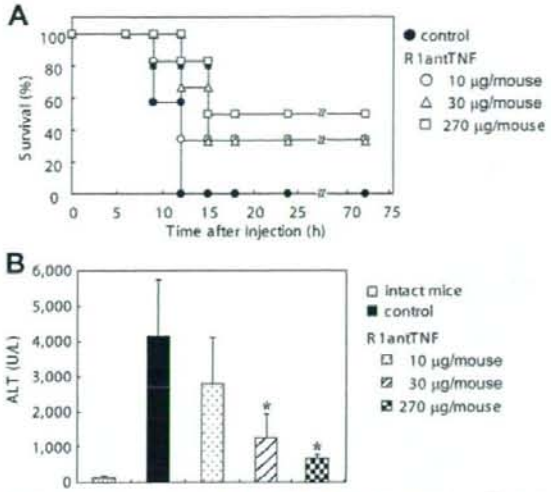

FIGURE 5. **Therapeutic effect of R1antTNF in lethal hepatitis model.** Mice were injected intravenously with recombinant human TNF (1.0 μg)/GalN (20 mg) and R1antTNF or PBS. *A*, survival rates of the mice in the TNF/GalN-induced hepatitis model were measured over a period of 72 h ($n = 6$). *B*, blood samples were collected 9 h after the challenge. Serum concentration of alanine aminotransferase (*ALT*) was measured as described under "Experimental Procedures" ($n = 6$). Data represent the mean ± S.E. Statistical significance *versus* control mice was calculated by unpaired Student's *t* test (*, $p < 0.05$).

TABLE 3
Binding properties of R1antTNF

Receptor	Kinetic parameter	wtTNF	R1antTNF
hTNFR1	k_{on} ($\times 10^5$ $M^{-1}s^{-1}$)[a]	3.6 ± 2.9	8.3 ± 0.1
	k_{off} ($\times 10^{-4}$ s^{-1})[b]	5.0 ± 1.3	28.7 ± 5.9
	K_D ($\times 10^{-9}$ M)[c]	1.4 ± 2.7	3.5 ± 1.8
hTNFR2	k_{on} ($\times 10^5$ $M^{-1}s^{-1}$)	7.0 ± 3.2	0.000001 ± 0.0
	k_{off} ($\times 10^{-4}$ s^{-1})	14.5 ± 4.9	0.1 ± 0.0
	K_D ($\times 10^{-9}$ M)	2.1 ± 1.1	92,900 ± 96.1
mTNFR1	k_{on} ($\times 10^5$ $M^{-1}s^{-1}$)	2.5 ± 0.0	18.7 ± 0.2
	k_{off} ($\times 10^{-4}$ s^{-1})	1.9 ± 0.3	96.6 ± 0.8
	K_D ($\times 10^{-9}$ M)	0.8 ± 0.4	5.2 ± 0.5

[a] k_{on} is the association kinetic constant.
[b] k_{off} is the dissociation kinetic constant.
[c] K_D is the equilibrium dissociation constant. Kinetic parameters for each TNF was calculated from the respective sensorgram by BIAevaluation 3.0 software.

performed using PC60-R1 and PC60-R2 cell lines that stably expressed hTNFR1 and hTNFR2 (25), respectively. R1antTNF efficiently inhibited the wtTNF-induced GM-CSF production in the PC60-R1 cells but not in the PC60-R2 cells (Fig. 4*C*), confirming the TNFR1-specific antagonistic activity. The risk of cross-activity to other TNF receptor superfamily members was assessed by Fas-induced cytotoxicity assay on Jurkat cell (Fig. 4*D*). R1antTNF did not affect the Fas-mediated signaling, which suggest that R1antTNF was highly selective proteo-antagonist of TNFR1. These data suggest that the R1antTNF not only binds to the TNFR1 selectively but also has TNFR1-selective inhibitory activity.

Therapeutic Efficacy of R1antTNF on Lethal Hepatitis Model—To assess the inhibitory activity and therapeutic effect of R1antTNF *in vivo*, we investigated the protective effect of R1antTNF in the TNF/D-(+)-galactosamine (GalN)-induced hepatitis model. GalN is a hepatotoxin that inhibits transcription and translation in hepatocytes. The combined administration of GalN and TNF causes massive apoptosis of hepatocytes and induces lethal hepatitis (36). In the control group, all mice died within 12 h after a lethal challenge with TNF/GalN (Fig. 5*A*). Co-treatment with R1antTNF improved the survival rate. Especially, in mice co-treated with R1antTNF (270 μg/mouse), the survival rates were 5/6 after 12 h and 3/6 after 24 h (Fig. 5*A*). The surviving mice were still alive several weeks after the treatment. In the control group, the serum levels of ALT, a marker for liver damage, were markedly elevated. In contrast, co-treatment of mice with R1antTNF suppressed the elevation of ALT levels in a dose-dependent manner (Fig. 5*B*). These results demonstrated that R1antTNF had antagonistic activity not only *in vitro* but also *in vivo*, and exhibited remarkable inhibitory effect on hepatitis.

Binding Mode and Affinity of R1antTNF—The dissociation constant (K_d) of R1antTNF binding to hTNFR1 was very similar to that of the wtTNF (Table 2), whereas the R1antTNF (mutTNF-T2) has no bioactivity through TNFR1 (Fig. 2*A*). We predicted that the binding modes of the wtTNF and R1antTNF to the TNFR1 are different, resulting in different biological activities. To quantify the altered binding mode of R1antTNF, we examined the binding kinetics of the R1antTNF for the mTNFR1, hTNFR1, and hTNFR2 using the surface plasmon resonance technique (Table 3). Indeed, the dissociation kinetic constants (k_{off}) of the R1antTNF for the human and mouse

TNFR1 (hTNFR1, $16.0 \times 10^{-4}\ s^{-1}$; mTNFR1, $37.0 \times 10^{-4}\ s^{-1}$) were clearly higher than those of the wtTNF (hTNFR1, $3.0 \times 10^{-4}\ s^{-1}$; mTNFR1, $1.5 \times 10^{-4}\ s^{-1}$). The association kinetic constants (k_{on}) of the R1antTNF for the human and mouse TNFR1 were also higher than those of the wtTNF. These results suggest that the R1antTNF interacts with the TNFR1 by repeating very quick binding and dissociation, and has a binding mode that is different from that of the wtTNF.

TABLE 4
X-ray data collection and refinement statistics (molecular replacement)

Crystal	R1antTNF
Data collection	
Space group	$P2_12_12_1$
Cell dimensions	
a, *b*, *c* (Å)	66.56, 66.97, 103.56
Resolution (Å)	50.0-1.80 (1.86-1.80)*
R_{merge}	0.063 (0.484)
$I/\sigma I$	36.8 (2.71)
Completeness (%)	99.6 (96.1)
Redundancy	7.1 (6.0)
Refinement	
Resolution (Å)	41.0-1.80
No. of reflections	42,155
R_{work}/R_{free}	19.8/23.9
No. of atoms	
Protein	3384
Water	237
Root mean squares deviations	
Bond lengths (Å)	0.00840
Bond angles (°)	1.47

* Highest resolution shell is shown in parentheses.

Crystal Structure of R1antTNF—To understand the structural basis for the different binding mode and absence of signal transduction via the R1antTNF, we examined the structure of R1antTNF by x-ray crystallography. After establishing crystallization conditions, good quality crystals of R1antTNF were obtained. The R1antTNF crystal size was $\sim 0.2 \times 0.2 \times 0.4\ mm^3$. X-ray diffraction data were collected in SPring-8 (the large synchrotron radiation facility in Japan). Analysis of these data show that the space group is $P2_12_12_1$, and the lattice constants are $a = 64.56$, $b = 66.97$, and $c = 103.56$ Å (Table 4). The R1antTNF structure was further refined using CNS. Results of the model validation using the Procheck were as follows: 88.4% residues in the most favored regions; 11.0% residues in the additional allowed regions; 0.6% residues in the generously allowed regions; and 0.0% residues in the disallowed regions. The overall structure of the R1antTNF was a trimer (Fig. 6*A*) (PDB code 2E7A), which was similar to that of the wtTNF trimer (Fig. 6*B*) (PDB code 1TNF) (37). Interestingly, structural superposition of the R1antTNF and human wtTNF showed extraordinary similarity (root mean square deviation 1.17 Å for 444 C-α atoms) of their overall structures despite their contradictory functions (Fig. 6*C*). It is believed that the TNF signaling is initiated by the formation of a complex with the three TNFRs on the cell surface. However, the fact that the R1antTNF did not transduce signaling suggests that there might be other structural differences between the wtTNF and R1antTNF.

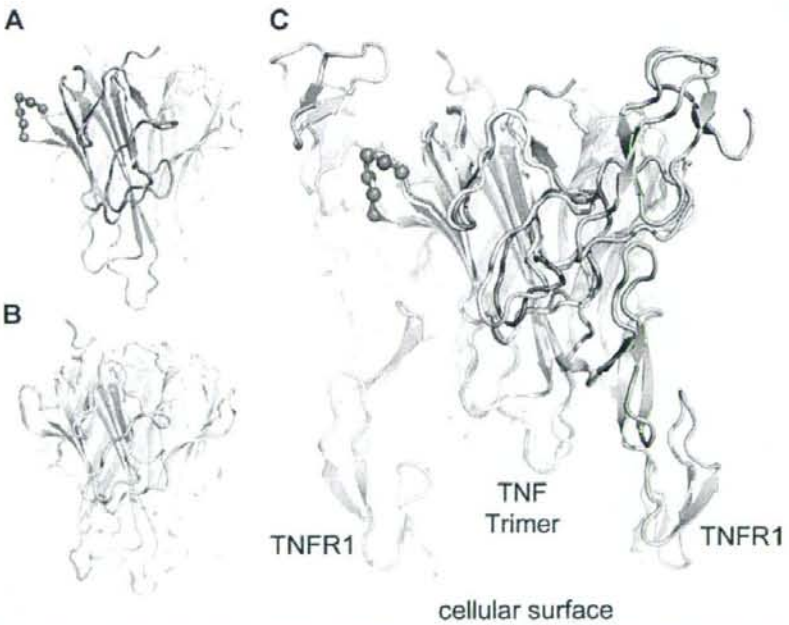

FIGURE 6. **Overall structures of R1antTNF and wtTNF.** *A*, refined structure of the R1antTNF trimer (*green*). *Blue spheres* show the mutated residues(amino acids 84–89) in R1antTNF. This structure is registered in the PDB (PDB code 2E7A). *B*, structure of the wtTNF trimer (*gray*). This structure has been published, and its PDB code is 1TNF. *C*, model structures of the TNF-TNFR1 complexes. Each TNF is superposed on the LT-α derived from the LT-α-TNFR1 complex (PDB code 1TNR). TNF binds to three R1 monomers on the cell surface. TNFR1s are shown using *red schematics*. Superposition of the structures of the wtTNF and R1antTNF was performed using the ccp4i program.

DISCUSSION

TNF, secreted from the site of injury or because of the activation of the immune cells, is involved in the development of inflammatory diseases, and it predominantly activates TNFR1 (40, 41). The TNFR1 knock-out mice have been reported to be resistant to the onset of several inflammatory diseases, such as sepsis, rheumatoid arthritis, and multiple sclerosis (14, 16, 42). In agreement with this, blocking the interaction between the TNF and TNFR1 has emerged as a powerful and clinically effective therapy for the acute inflammation and autoimmune conditions. In this study, we generated TNFR1-selective antagonistic TNF mutants using a phage library displaying structural variants of human TNF.

Among 10 potential candidates, the mutTNF-T2 (R1antTNF) selectively and strongly bound to the TNFR1 but showed almost no bioactivity. Additionally, we found that R1antTNF most effectively inhibited the wtTNF-induced cell death

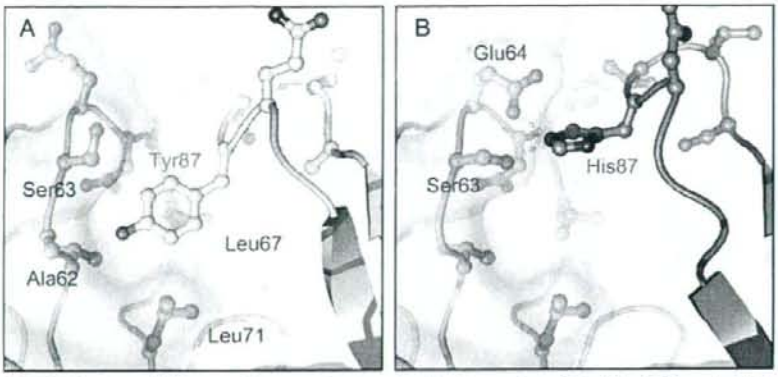

FIGURE 7. **Structural difference between the receptor binding region of the R1antTNF and wtTNF.** *A*, interaction between the wtTNF (*gray*) and TNFR1 (*red*). *White layer* depicts the molecular surface of the TNFR1. Hydrophobic interaction is formed between the Tyr-87 and molecular pocket in the TNFR1 (Leu-67, Leu-71, Ala-62, and Ser-63). *B*, interaction between the R1antTNF (*green*) and TNFR1 (*red*). *Yellow broken lines* show the possible interactions of the R1antTNF His-87 with the receptor Ser-63 and Glu-64. In this simulation, the side chains of each structure were rotated to fit the predicted interaction. Stable structures of these rotamers were constructed using the O program.

(Fig. 3*B*). R1antTNF also clearly inhibited the TNF functions other than cytotoxicity. Interestingly, the ratio between the R1antTNF and wtTNF was 1000-fold or more to obtain 50% inhibition against the wtTNF-induced cytotoxicity and caspase-3/7 activity, whereas the ratio was only about 100-fold or less to obtain 50% inhibition against the wtTNF-induced expression of E-selectin, production of GM-CSF, and NF-κB activation. Intracellular signaling induced by the TNF/TNFR1 interaction is divided into the following two main pathways: (i) the NF-κB pathway, which regulates the expression of adhesion molecules and inflammatory cytokines, and (ii) the caspase cascade, which induces cell death through apoptosis or necrosis (34). Our results suggest that R1antTNF is more antagonistic against the wtTNF function mediated via the NF-κB pathway than via the caspase cascade. In pathological tissues, endogenous TNF induced expression of the cell adhesion molecules and inflammatory cytokines resulting in leukocyte infiltration, which are regulated by NF-κB and are closely related to the development or exacerbation of diseases (43) such as fulminant hepatitis and rheumatoid arthritis. Because the R1antTNF efficiently inhibited the TNF-induced NF-κB activation, it would be of therapeutic value for the treatment of such inflammatory diseases. These cell line or signaling pathway-dependent differences in the inhibitory efficiencies of R1antTNF could be valuable in studying the structural or biological changes caused by the TNF/TNFR1 interactions, which need to be explored further.

We examined the therapeutic effects of R1antTNF in the acute lethal hepatitis model. R1antTNF exhibited the suppressive effect on acute hepatitis. Although the R1antTNF suppressed the elevation of the ALT level in a dose-dependent manner, the survival rate was not significantly improved between the dose 10 μg/mouse *versus* 270 μg/mouse. This discrepancy is likely because the difference in the degree of suppression of the elevated ALT level does not always correlate well with the improvement in the survival rate. Nevertheless, treatment with only 30–270 μg/mouse R1antTNF (30–270-fold excess over wtTNF) significantly suppressed the elevation of ALT levels and reduced the lethal toxicity. Thus, the antagonistic activity of R1antTNF *in vivo* was stronger than expected from the *in vitro* results. The TNF/GalN-mediated activation of TNFR1 not only induces apoptosis and necrosis of hepatocytes but also induces inflammatory responses and secondary responses associated with the cell death (44). Therefore, we believe that the R1antTNF exerted its therapeutic effect by comprehensively inhibiting the TNF/GalN-mediated biological responses, thus blocking the liver failure in the experimental animals. The R1antTNF is also expected to have therapeutic effect in chronic inflammatory disease models, such as in collagen-induced arthritis model and experimental autoimmune encephalomyelitis model. However, the plasma half-life of R1antTNF, like the wtTNF, is very short (12 min). We recently developed a novel PEGylation system that dramatically improved the *in vivo* stability and therapeutic effects of the bioactive proteins (29, 45). We are currently in the process of developing the PEGylated R1antTNF to further enhance its potential anti-inflammatory activity.

To explore the underlying mechanism of the antagonistic activity of R1antTNF, we examined the crystal structure of R1antTNF by x-ray crystallography. Despite close resemblance between the crystal structure of the R1antTNF and wtTNF, the receptor-bound R1antTNF did not transmit any signal via the TNFR1. To further speculate why the R1antTNF showed antagonistic activity, we utilized the superpose program to perform docking simulations with the TNFs and TNFR1 using the crystal structure of the LT-α-TNFR1 complex (PDB code 1TNR) (31). The TNF-TNFR1 model complex suggested that the Tyr-87 of the wtTNF, an essential residue, is buried in a molecular hydrophobic "pocket" of the TNFR1, which houses the receptor residues Leu-67 and Leu-71 that are implicated to maintain the TNF and TNFR1 complex (Fig. 7*A*). Tyr-87 is a highly conserved residue throughout the TNF superfamily, such as LT-α, LT-β and LIGHT, and this discussion is also reflected in the crystal structure of the LT-α-TNFR1 complex (38). Accordingly, site-directed mutagenesis of the Tyr-87 residue of TNF resulted in a dramatic loss of its biological activity and affinities for both TNFRs (39), suggesting that this residue is be essential for TNF function. However, in R1antTNF, the Tyr-87 is replaced with a histidine residue. The structural simulation studies suggested that the His-87 in R1antTNF could interact with the relatively negatively charged Ser-63 and Glu-64 residues on the TNFR1 surface, which probably explains the different binding mode of the R1antTNF as compared with the wtTNF (Fig. 7*B*).

Indeed, the association and dissociation kinetic constants (k_{on} and k_{off}, respectively) for the binding of R1antTNF to TNFR1 were considerably higher than those of the wtTNF, indicating a difference in the TNFR1-binding pattern between the wtTNF and R1antTNF (Table 3). The association and dissociation kinetic constants are very important factors in discussing the ligand-receptor interaction and function. It was previously shown that the membrane-bound TNF, but not the soluble TNF, could activate the TNFR2, and the reason for this difference was attributed to the dissociation kinetic constant of the soluble TNF, which was much higher than the membrane-bound TNF (46). Therefore, the inability of R1antTNF to transmit signal and its antagonistic activity are probably because of the higher k_{on} and k_{off} values of R1antTNF for the TNFR1, suggesting that they influenced the stability of the TNF-TNFR1 complex and reduced the continuous binding time required for the signal transmission. In addition, we demonstrated that R1antTNF inhibited the activations of both caspase-3/7 and NF-κB (Fig. 5, *A* and *B*), which are mediated via two distinct intracellular signaling complexes. TNF/TNFR1-mediated signaling requires sequential formation of the following two receptor complexes: the complex I is involved in the recruitment of TRADD, RIP1, and TRAF2 leading to the NF-κB activation, whereas the consequent complex II is involved in internalization, post-translational modifications, and recruitment of FADD and caspase-8 initiating apoptosis (47). Together, these results suggest that R1antTNF blocked the TNF-mediated signal transmission by binding to TNFR1 in a rapid association/dissociation cycle, thereby inhibiting the formation of the intracellular complexes. However, more detailed investigations, such as detection of these intracellular complexes and their internalization, other TNF/TNFR1-mediated signaling, and analysis of the complex structure of the R1antTNF and TNFR1, are required to elucidate exactly how the R1antTNF exhibits its TNFR1 antagonistic activity.

We succeeded in developing the first mutant form of the human TNF with TNFR1-selective antagonistic activity by using a unique combinatorial phage-based technique. Existing TNF blockers, *i.e.* etanercept and infliximab, are widely used in the treatment of rheumatoid arthritis and Crohn disease (5). But these drugs, which prevent TNF binding on both TNF receptor types, can cause serious side effects, such as mycobacterial infections and hepatitis B virus infection (48). Although TNFR1 is believed to be important for immunological responses (42), TNFR2 is thought to be also important for antiviral resistance and is effective for controlling the mycobacterial infection by affecting the membrane-bound TNF stimulation (18, 49). Therefore, this mutant TNF, R1antTNF, might be a new therapeutic drug with reduced side effects. We are currently evaluating not only the therapeutic effect of R1antTNF on rheumatoid arthritis or experimental encephalomyelitis model, and but also its side effects such as mycobacterial and virus infection. Finally, our studies demonstrate the feasibility of generating TNF receptor subtype-selective antagonistic mutants by comprehensive substitution of sets of amino acids in the wild-type ligand proteins. Our data also suggest that this combinatorial biosynthetic strategy using the bioactive protein as the "lead protein" is very effective in creating receptor-specific agonists and antagonists, and we believe that this approach will generate protein drugs of improved therapeutic value.

Acknowledgment—We thank E. C. Gabazza for discussions and critical reading of the manuscript.

REFERENCES

1. Aggarwal, B. B. (2003) *Nat. Rev. Immunol.* **3,** 745–756
2. Aderka, D., Engelmann, H., Maor, Y., Brakebusch, C., and Wallach, D. (1992) *J. Exp. Med.* **175,** 323–329
3. Feldmann, M., and Maini, R. N. (2003) *Nat. Med.* **9,** 1245–1250
4. Muto, Y., Nouri-Aria, K. T., Meager, A., Alexander, G. J., Eddleston, A. L., and Williams, R. (1988) *Lancet* **2,** 72–74
5. Feldmann, M. (2002) *Nat. Rev. Immunol.* **2,** 364–371
6. Goldbach-Mansky, R., and Lipsky, P. E. (2003) *Annu. Rev. Med.* **54,** 197–216
7. Brown, S. L., Greene, M. H., Gershon, S. K., Edwards, E. T., and Braun, M. M. (2002) *Arthritis Rheum.* **46,** 3151–3158
8. Keane, J., Gershon, S., Wise, R. P., Mirabile-Levens, E., Kasznica, J., Schwieterman, W. D., Siegel, J. N., and Braun, M. M. (2001) *N. Engl. J. Med.* **345,** 1098–1104
9. Nathan, D. M., Angus, P. W., and Gibson, P. R. (2006) *J. Gastroenterol. Hepatol.* **21,** 1366–1371
10. Shakoor, N., Michalska, M., Harris, C. A., and Block, J. A. (2002) *Lancet* **359,** 579–580
11. Sicotte, N. L., and Voskuhl, R. R. (2001) *Neurology* **57,** 1885–1888
12. Aggarwal, B. B., Eessalu, T. E., and Hass, P. E. (1985) *Nature* **318,** 665–667
13. Leist, M., Gantner, F., Jilg, S., and Wendel, A. (1995) *J. Immunol.* **154,** 1307–1316
14. Mori, L., Iselin, S., De Libero, G., and Lesslauer, W. (1996) *J. Immunol.* **157,** 3178–3182
15. Liu, J., Marino, M. W., Wong, G., Grail, D., Dunn, A., Bettadapura, J., Slavin, A. J., Old, L., and Bernard, C. C. (1998) *Nat. Med.* **4,** 78–83
16. Kassiotis, G., and Kollias, G. (2001) *J. Exp. Med.* **193,** 427–434
17. Fremond, C., Allie, N., Dambuza, I., Grivennikov, S. I., Yeremeev, V., Quesniaux, V. F., Jacobs, M., and Ryffel, B. (2005) *Respir. Res.* **6,** 136
18. Olleros, M. L., Guler, R., Corazza, N., Vesin, D., Eugster, H. P., Marchal, G., Chavarot, P., Mueller, C., and Garcia, I. (2002) *J. Immunol.* **168,** 3394–3401
19. Grell, M., Becke, F. M., Wajant, H., Mannel, D. N., and Scheurich, P. (1998) *Eur. J. Immunol.* **28,** 257–263
20. Kafrouni, M. I., Brown, G. R., and Thiele, D. L. (2003) *J. Leukocyte Biol.* **74,** 564–571
21. Kim, E. Y., Priatel, J. J., Teh, S. J., and Teh, H. S. (2006) *J. Immunol.* **176,** 1026–1035
22. Engelmann, H., Holtmann, H., Brakebusch, C., Avni, Y. S., Sarov, I., Nophar, Y., Hadas, E., Leitner, O., and Wallach, D. (1990) *J. Biol. Chem.* **265,** 14497–14504
23. Carter, P. H., Scherle, P. A., Muckelbauer, J. K., Voss, M. E., Liu, R. Q., Thompson, L. A., Tebben, A. J., Solomon, K. A., Lo, Y. C., Li, Z., Strzemienski, P., Yang, G., Falahatpisheh, N., Xu, M., Wu, Z., Farrow, N. A., Ramnarayan, K., Wang, J., Rideout, D., Yalamoori, V., Domaille, P., Underwood, D. J., Trzaskos, J. M., Friedman, S. M., Newton, R. C., and Decicco, C. P. (2001) *Proc. Natl. Acad. Sci. U. S. A.* **98,** 11879–11884
24. Murali, R., Cheng, X., Berezov, A., Du, X., Schon, A., Freire, E., Xu, X., Chen, Y. H., and Greene, M. I. (2005) *Proc. Natl. Acad. Sci. U. S. A.* **102,** 10970–10975
25. Vandenabeele, P., Declercq, W., Vercammen, D., Van de Craen, M., Grooten, J., Loetscher, H., Brockhaus, M., Lesslauer, W., and Fiers, W. (1992) *J. Exp. Med.* **176,** 1015–1024
26. Tsutsumi, Y., Kihira, T., Tsunoda, S., Kanamori, T., Nakagawa, S., and Mayumi, T. (1995) *Br. J. Cancer* **71,** 963–968
27. Barbara, J. A., Smith, W. B., Gamble, J. R., Van Ostade, X., Vandenabeele,

P., Tavernier, J., Fiers, W., Vadas, M. A., and Lopez, A. F. (1994) *EMBO J.* **13,** 843–850
28. Brunetti, C. R., Paulose-Murphy, M., Singh, R., Qin, J., Barrett, J. W., Tardivel, A., Schneider, P., Essani, K., and McFadden, G. (2003) *Proc. Natl. Acad. Sci. U. S. A.* **100,** 4831–4836
29. Yamamoto, Y., Tsutsumi, Y., Yoshioka, Y., Nishibata, T., Kobayashi, K., Okamoto, T., Mukai, Y., Shimizu, T., Nakagawa, S., Nagata, S., and Mayumi, T. (2003) *Nat. Biotechnol.* **21,** 546–552
30. Potterton, E., Briggs, P., Turkenburg, M., and Dodson, E. (2003) *Acta Crystallogr. Sect. D. Biol. Crystallogr.* **59,** 1131–1137
31. Banner, D. W., D'Arcy, A., Janes, W., Gentz, R., Schoenfeld, H. J., Broger, C., Loetscher, H., and Lesslauer, W. (1993) *Cell* **73,** 431–445
32. Jones, T. A., Zou, J. Y., Cowan, S. W., and Kjeldgaard, M. (1991) *Acta Crystallogr. Sect. A.* **47,** 110–119
33. Brunger, A. T., Adams, P. D., Clore, G. M., DeLano, W. L., Gros, P., Grosse-Kunstleve, R. W., Jiang, J. S., Kuszewski, J., Nilges, M., Pannu, N. S., Read, R. J., Rice, L. M., Simonson, T., and Warren, G. L. (1998) *Acta Crystallogr. Sect. D. Biol. Crystallogr.* **54,** 905–921
34. Chen, G., and Goeddel, D. V. (2002) *Science* **296,** 1634–1635
35. Mackay, F., Loetscher, H., Stueber, D., Gehr, G., and Lesslauer, W. (1993) *J. Exp. Med.* **177,** 1277–1286
36. Hishinuma, I., Nagakawa, J., Hirota, K., Miyamoto, K., Tsukidate, K., Yamanaka, T., Katayama, K., and Yamatsu, I. (1990) *Hepatology* **12,** 1187–1191
37. Eck, M. J., and Sprang, S. R. (1989) *J. Biol. Chem.* **264,** 17595–17605
38. Harrop, J. A., McDonnell, P. C., Brigham-Burke, M., Lyn, S. D., Minton, J., Tan, K. B., Dede, K., Spampanato, J., Silverman, C., Hensley, P., DiPrinzio, R., Emery, J. G., Deen, K., Eichman, C., Chabot-Fletcher, M., Truneh, A., and Young, P. R. (1998) *J. Biol. Chem.* **273,** 27548–27556
39. Zhang, X. M., Weber, I., and Chen, M. J. (1992) *J. Biol. Chem.* **267,** 24069–24075
40. Ruuls, S. R., Hoek, R. M., Ngo, V. N., McNeil, T., Lucian, L. A., Janatpour, M. J., Korner, H., Scheerens, H., Hessel, E. M., Cyster, J. G., McEvoy, L. M., and Sedgwick, J. D. (2001) *Immunity* **15,** 533–543
41. Grell, M., Douni, E., Wajant, H., Lohden, M., Clauss, M., Maxeiner, B., Georgopoulos, S., Lesslauer, W., Kollias, G., Pfizenmaier, K., and Scheurich, P. (1995) *Cell* **83,** 793–802
42. Rothe, J., Lesslauer, W., Lotscher, H., Lang, Y., Koebel, P., Kontgen, F., Althage, A., Zinkernagel, R., Steinmetz, M., and Bluethmann, H. (1993) *Nature* **364,** 798–802
43. Zhou, A., Scoggin, S., Gaynor, R. B., and Williams, N. S. (2003) *Oncogene* **22,** 2054–2064
44. Nagaki, M., Sugiyama, A., Osawa, Y., Naiki, T., Nakashima, S., Nozawa, Y., and Moriwaki, H. (1999) *J. Hepatol.* **31,** 997–1005
45. Kamada, H., Tsutsumi, Y., Sato-Kamada, K., Yamamoto, Y., Yoshioka, Y., Okamoto, T., Nakagawa, S., Nagata, S., and Mayumi, T. (2003) *Nat. Biotechnol.* **21,** 399–404
46. Krippner-Heidenreich, A., Tubing, F., Bryde, S., Willi, S., Zimmermann, G., and Scheurich, P. (2002) *J. Biol. Chem.* **277,** 44155–44163
47. Micheau, O., and Tschopp, J. (2003) *Cell* **114,** 181–190
48. Gomez-Reino, J. J., Carmona, L., Valverde, V. R., Mola, E. M., and Montero, M. D. (2003) *Arthritis Rheum.* **48,** 2122–2127
49. Saunders, B. M., Tran, S., Ruuls, S., Sedgwick, J. D., Briscoe, H., and Britton, W. J. (2005) *J. Immunol.* **174,** 4852–4859

British Journal of Pharmacology (2008), 1–10

0007–1188/08 $30.00
www.brjpharmacol.org

RESEARCH PAPER

Comparative study on transduction and toxicity of protein transduction domains

T Sugita[1,2], T Yoshikawa[1], Y Mukai[1,2], N Yamanada[1,2], S Imai[1,2], K Nagano[1,2], Y Yoshida[1,3], H Shibata[1], Y Yoshioka[1,4], S Nakagawa[2], H Kamada[1,4], S-i Tsunoda[1,4] and Y Tsutsumi[1,3,4]

[1]*Laboratory of Pharmaceutical Proteomics, National Institute of Biomedical Innovation (NIBIO), Ibaraki, Osaka, Japan;* [2]*Department of Biotechnology and Therapeutics, Graduate School of Pharmaceutical Sciences, Osaka University, Suita, Osaka, Japan;* [3]*Department of Biomedical Innovation, Graduate School of Pharmaceutical Sciences, Osaka University, Suita, Osaka, Japan and* [4]*The Center for Advanced Medical Engineering and Informatics, Osaka University, Suita, Osaka, Japan*

Background and purpose: Protein transduction domains (PTDs), such as Tat, antennapedia homeoprotein (Antp), Rev and VP22, have been extensively utilized for intracellular delivery of biologically active macromolecules *in vitro* and *in vivo*. There is little known, however, about the relative transduction efficacy, cytotoxicity and internalization mechanism of individual PTDs.
Experimental approach: We examined the cargo delivery efficacies of four major PTDs (Tat, Antp, Rev and VP22) and evaluated their toxicities and cell internalizing pathways in various cell lines.
Key results: The relative order of the transduction efficacy of these PTDs conjugated to fluorescein was Rev>Antp>Tat>VP22, independent of cell type (HeLa, HaCaT, A431, Jurkat, MOLT-4 and HL60 cells). Antp produced significant toxicity in HeLa and Jurkat cells, and Rev produced significant toxicity in Jurkat cells. Flow cytometric analysis demonstrated that the uptake of PTD–fluorescein conjugate was dose-dependently inhibited by methyl-β-cyclodextrin, cytochalasin D and amiloride, indicating that all four PTDs were internalized by the macropinocytotic pathway. Accordingly, in cells co-treated with 'Tat-fused' endosome-disruptive HA2 peptides (HA2-Tat) and independent PTD-fluorescent protein conjugates, fluorescence spread throughout the cytosol, indicating that all four PTDs were internalized into the same vesicles as Tat.
Conclusions and implications: These findings suggest that macropinocytosis-dependent internalization is a crucial step in PTD-mediated molecular transduction. From the viewpoint of developing effective and safe protein transduction technology, although Tat was the most versatile carrier among the peptides studied, PTDs should be selected based on their individual characteristics.
British Journal of Pharmacology advance online publication, 28 January 2008; doi:10.1038/sj.bjp.0707678

Keywords: protein transduction domains; Tat; antennapedia; Rev; VP22; macropinocytosis

Abbreviations: PTD, protein transduction domain; Antp, antennapedia

Introduction

A strong focus of research in the post-genomic era is the development of effective therapies for refractory diseases such as cancer and neurodegenerative syndromes (Rhodes and Chinnaiyan, 2005; Brusic *et al.*, 2007; Drabik *et al.*, 2007). Because the therapeutic targets of these diseases generally exist inside the cell, it is necessary to establish drug delivery methods that transfer macromolecules, such as therapeutic proteins or peptide-based drugs, across the cellular membrane (Nori and Kopecek, 2005; Murriel and Dowdy, 2006; Borsello and Forloni, 2007).

Correspondence: Dr S-i Tsunoda, Laboratory of Pharmaceutical Proteomics, National Institute of Biomedical Innovation (NIBIO), 7-6-8 Saito-Asagi, Ibaraki, Osaka 597-0085, Japan.
E-mail: tsunoda@nibio.go.jp
Received 9 November 2007; accepted 4 December 2007

Protein transduction is a recently developed method for delivering biologically active proteins directly into mammalian cells with high efficiency (Hawiger, 1999; Schwarze *et al.*, 2000). Recombinant technology is used to modify the biophysical properties of proteins and peptides, particularly with respect to their cell permeability, using the so-called protein transduction domains (PTDs) (Nagahara *et al.*, 1998; Rojas *et al.*, 1998; Schwarze *et al.*, 1999). The HIV-1-derived Tat peptide renders various macromolecules cell permeable. Although the initial reports suggested that protein transduction is energy and temperature independent, these characteristics are now mostly attributed to phenomena such as fixation artefacts (Richard *et al.*, 2003). More recent data indicate that basic PTDs such as Tat enter the cells through a macropinocytotic pathway that is universally active in all cells (Wadia *et al.*, 2004; Kaplan *et al.*, 2005). A series of events involves Tat attachment to an anionic cell surface,

followed by the association of these complexes with lipid rafts, which triggers dynamin-independent macropinocytosis. After internalization, the endosome pH falls and Tat apparently destabilizes the membranes, which results in a small amount of the endosome contents escaping into the cytosol. The released fraction of Tat can then exert its biologic activity. Consistent with this model, Tat delivery is enhanced by the influenza virus haemagglutinin fusogenic motif, which further destabilizes endosomal membranes at a low pH (Han *et al.*, 2001; Skehel *et al.*, 2001). In cells cotreated with Tat-conjugated HA2 (HA2-Tat), a greater proportion of endocytosed Tat-fused Cre recombinase escapes into the cytoplasm (Wadia *et al.*, 2004). Other studies suggest that certain cell types might incorporate Tat constructs by clathrin- or caveolin-dependent endocytosis, raising the possibility that transport varies according to the cargo or cell type (Ferrari *et al.*, 2003; Fittipaldi *et al.*, 2003; Richard *et al.*, 2005). In addition to the basic Tat peptide, there are other proteins (fragments), such as antennapedia (Antp), Rev and VP22, that enhance cellular uptake of proteins (Table 1) (Derossi *et al.*, 1994; Elliott and O'Hare, 1997; Futaki *et al.*, 2001; Joliot and Prochiantz, 2004). These four well-known PTDs facilitate the delivery of various biomacromolecules into the cell, but few studies have examined their relative efficacy.

In the present study, we evaluated the potency and internalizing pathway of four major PTDs to optimize protein transduction technology and to clarify the mechanisms of action. We also evaluated the cytotoxicity of these four PTDs as this is crucial to their utility as effective biomacromolecule carriers. These analyses may help not only to elucidate the mechanism by which the four peptides facilitate the cellular uptake of biomacromolecules, but also provide criteria for their proper use.

Materials and methods

Cell lines

HeLa cells (human cervical carcinoma cells) and A431 cells (human epithelial carcinoma cells) were obtained from the American Type Culture Collection (Manassas, VA, USA). HaCaT cells (human keratinocyte cells) were kindly provided by Dr S Inui, Osaka University. Jurkat cells (human leukaemia cells) and MOLT-4 cells (human leukaemia cells) were kindly provided by Hayashibara Biochemical Laboratories Inc. (Okayama, Japan). HL60 cells (human promyelocytic leukaemia cells) were obtained from the Japanese Collection of Research Bioresources (JCRB; Osaka, Japan). HeLa cells were cultured in minimal essential medium (MEMα; Wako Pure Chemicals, Osaka, Japan) medium supplemented with 10% fetal bovine serum (FBS) and antibiotics. A431 cells and HaCaT cells were maintained in Dulbecco's modified Eagle's medium (Wako Pure Chemicals) supplemented with 10% FBS, 1% L-glutamine and antibiotics. Jurkat cells and MOLT-4 cells were maintained in RPMI-1640 medium (Wako Pure Chemicals) supplemented with 10% FBS and antibiotics. HL60 cells were maintained in RPMI-1640 medium (Wako Pure Chemicals) supplemented with 20% FBS and antibiotics. All cells were cultured at 37 °C in 5% CO_2.

Table 1 Protein sequences of the PTDs evaluated

PTD	*Origin*	*Sequence*	*pI*
Tat	HIV-1	GRKKRRQRRRPPQ	12.70
Antp	*Drosophila*	RQIKIWFQNRRMKWKK	12.31
Rev	HIV-1	TRQARRNRRRRWRERQF	12.60
VP22	HSV	NAKTRRHERRRKLAIER	12.01

The basic amino acids in each sequence are shown in bold.

Synthetic peptides

All peptides used in this study were purchased from the Toray Research Center Inc. (Tokyo, Japan) and had purities above 90%, which was confirmed by high-performance liquid chromatography analysis and mass spectroscopy. The sequences of these peptides were GRKKRRQRRRPPQK-FAM (FAM = carboxyfluorescein) for Tat-conjugated FAM (Tat-FAM), RQIKIWFQNRRMKWKKK-FAM for Antp-conjugated FAM (Antp-FAM), TRQARRNRRRRWRERQRK-FAM for Rev-conjugated FAM (Rev-FAM), NAKTRRHERRRKLAIERK-FAM for VP22-conjugated FAM (VP22-FAM), YGRKKRRQRRRK-biotin for Tat-conjugated biotin, RQIKIWFQNRRMKWKKK-biotin Antp-conjugated biotin, TQRARRNRRRRWRERQRK-biotin for Rev-conjugated biotin, NAKTRRHERRRKLAIERK-biotin for VP22-conjugated biotin and GLFEAIEGFIENGWEGMIDGWY GYGRKKRRQRRR for HA2-conjugated Tat (HA2-Tat). The individual PTD sequences are underlined.

Flow cytometric analysis

HeLa cells, HaCaT cells and A431 cells were cultured in 24-well plates (Nalge Nunc International, Naperville, IL, USA) at 5.0×10^4 cells per well in culture medium and incubated for 24 h at 37 °C. Jurkat cells, MOLT-4 cells and HL60 cells were cultured in 24-well plates (Nalge Nunc International) at 1.0×10^5 cells per well in Opti-MEM I (Invitrogen, Carlsbad, CA, USA). After aspirating the media, FAM-conjugated PTD (PTD-FAM) (10 μM) was added to the cells in Opti-MEM I and the culture dishes were incubated for an additional 3 h. Following incubation, the cells were washed with phosphate-buffered saline and incubated for 5 min with 0.1% trypsin to detach them and to remove surface-bound peptides. After incubation, 2 vol of 10% FBS-containing culture medium was added to stop the trypsin activity and to detach the cells completely. The cell suspension was centrifuged at 800 *g*, washed with phosphate-buffered saline, centrifuged again and resuspended in 500 μl of 0.4% paraformaldehyde. Fluorescence was analysed on a FACSCalibur flow cytometer, and data were analysed using CellQuest software (both from Becton Dickinson, San Jose, CA, USA). In the low-temperature uptake experiment, cells were preincubated at 4 °C for 1 h in Opti-MEM I prior to adding the PTDs, and all buffers and solutions were equilibrated to 4 °C. To analyse the internalization mechanism, HeLa cells were pretreated for 30 min in Opti-MEM I medium with 0–5 mM methyl-β-cyclodextrin, 0–2.5 μM